ARMY RESEARCH LABORATORY

Analytical Solutions for the Resonance Response of Goupillaud-type Elastic Media Using Z-transform Methods

by G. A. Gazonas and A. P. Velo

ARL-RP-353 **February 2012**

A reprint from *Wave Motion*, vol. 49, pp. 135–151, 2012.

NOTICES

Disclaimers

The findings in this report are not to be construed as an official Department of the Army position unless so designated by other authorized documents.

Citation of manufacturer's or trade names does not constitute an official endorsement or approval of the use thereof.

Destroy this report when it is no longer needed. Do not return it to the originator.

Army Research Laboratory
Aberdeen Proving Ground, MD 21005-5069

ARL-RP-353 **February 2012**

Analytical Solutions for the Resonance Response of Goupillaud-type Elastic Media Using Z-transform Methods

G. A. Gazonas
Weapons and Materials Research Directorate, ARL

A. P. Velo
University of San Diego

A reprint from *Wave Motion*, Vol. 49, pp. 135–151, 2012.

REPORT DOCUMENTATION PAGE

Form Approved
OMB No. 0704-0188

1. REPORT DATE *(DD-MM-YYYY)*	2. REPORT TYPE	3. DATES COVERED (From - To)
February 2012	Reprint	January 2010–March 2011

4. TITLE AND SUBTITLE
Analytical Solutions for the Resonance Response of Goupillaud-type Elastic Media Using Z-transform Methods

5a. CONTRACT NUMBER

5b. GRANT NUMBER

5c. PROGRAM ELEMENT NUMBER

6. AUTHOR(S)
George A. Gazonas and A. P. Velo*

5d. PROJECT NUMBER
AH42

5e. TASK NUMBER

5f. WORK UNIT NUMBER

7. PERFORMING ORGANIZATION NAME(S) AND ADDRESS(ES)
U.S. Army Research Laboratory
ATTN: RDRL-WMM-B
Aberdeen Proving Ground, MD 21005-5069

8. PERFORMING ORGANIZATION REPORT NUMBER
ARL-RP-353

9. SPONSORING/MONITORING AGENCY NAME(S) AND ADDRESS(ES)

10. SPONSOR/MONITOR'S ACRONYM(S)

11. SPONSOR/MONITOR'S REPORT NUMBER(S)

12. DISTRIBUTION/AVAILABILITY STATEMENT
Approved for public release; distribution is unlimited.

13. SUPPLEMENTARY NOTES
A reprint from *Wave Motion*, vol. 49, pp. 135–151, 2012.

*Department of Mathematics and Computer Science, University of San Diego, 5998 Alcalá Park, San Diego, CA 92110

14. ABSTRACT
The resonance frequency spectrum is derived for an m-layered Goupillaud medium subjected to a discrete sinusoidal forcing function that varies harmonically with time at one end with the other end held fixed. Analytical stress solutions are derived from a coupled first-order system of difference equations using z-transform methods. The determinant of the resulting global system matrix in the z-space $|\mathbf{A_m}|$ is a palindromic polynomial with real coefficients. The zeros of the palindromic polynomial are distinct and are proven to lie on the unit circle for $1 \leq m \leq 5$ and for certain classes of multilayered designs identified by tridiagonal Toeplitz matrices. An important result is the physical interpretation that all the positive angles, coterminal with the angles corresponding to the zeros of $|\mathbf{A_m}|$ on the unit circle, represent the resonance frequency spectrum for the discrete model. A sequence of resonance frequencies for the discrete model is universal (independent of design parameters) for all multilayered designs with an odd number of layers. The discrete model resonance frequency results are also extended to describe the resonance frequency spectrum for a continuous model. Results show that the natural frequency spectrum depends on the layer impedance ratios and are inversely proportional to the equal wave travel time for each layer.

15. SUBJECT TERMS
stress amplitude, palindromic polynomials, travel-time variable, Chebyshev polynomial, natural frequency formula, analog-to-digital conversion, Goupillad-type layered media, wave propagation

16. SECURITY CLASSIFICATION OF:			17. LIMITATION OF ABSTRACT	18. NUMBER OF PAGES	19a. NAME OF RESPONSIBLE PERSON
a. REPORT	b. ABSTRACT	c. THIS PAGE			George A. Gazonas
Unclassified	Unclassified	Unclassified	UU	26	19b. TELEPHONE NUMBER (*Include area code*) 410-306-0863

Wave Motion 49 (2012) 135–151

Contents lists available at SciVerse ScienceDirect

Wave Motion

journal homepage: www.elsevier.com/locate/wavemoti

Analytical solutions for the resonance response of Goupillaud-type elastic media using z-transform methods

G.A. Gazonas [a,*], A.P. Velo [b]

[a] US Army Research Laboratory, Weapons and Materials Research Directorate, Aberdeen Proving Ground, MD 21005, USA
[b] Department of Mathematics and Computer Science, University of San Diego, 5998 Alcalá Park, San Diego, CA 92110, USA

ARTICLE INFO

Article history:
Received 14 March 2011
Received in revised form 1 August 2011
Accepted 5 August 2011
Available online 19 August 2011

Keywords:
Stress amplitude
Palindromic polynomials
Travel-time variable
Chebyshev polynomial
Natural frequency formula
Analog to digital conversion

ABSTRACT

The resonance frequency spectrum is first derived for an m-layered Goupillaud-type elastic medium that is subjected to a discrete sinusoidal forcing function that varies harmonically with time at one end and held fixed at the other end. Analytical stress solutions are obtained from a coupled first-order system of difference equations using z-transform methods, where the determinant of the resulting global system matrix in the z-space $|\mathbf{A_m}|$ is a palindromic polynomial with real coefficients. The zeros of the palindromic polynomial are distinct and are proven to lie on the unit circle for $1 \leq m \leq 5$ and for certain classes of multilayered designs identified by tridiagonal Toeplitz matrices. An important result is the physical interpretation that all the positive angles, coterminal with the angles corresponding to the zeros of $|\mathbf{A_m}|$ on the unit circle, represent the resonance frequency spectrum for the discrete model. A sequence of resonance frequencies for the discrete model appears to be universal for all multilayered designs with an odd number of layers, as it is independent of any design parameters.

The resonance frequency results for the discrete model are then extended to describe the resonance frequency spectrum for the continuous model, where the forcing function applied at one end of the strip is continuous and varies harmonically with time while the other end is held fixed. The proposed natural frequency spectrum for a free-fixed m-layered Goupillaud-type strip is confirmed by independently solving a simplified form of the frequency equation, obtained after applying a transformation of the spatial variable. Our results suggest that the natural frequency spectrum depends on the layer impedance ratios and it is inversely proportional to the equal wave travel time for each layer.

The results are used to identify layered designs with a common frequency spectrum and modify an existing design to obtain a desired frequency spectrum. Other connections are made with previous stress optimization results, the Chebyshev polynomials of the first and second kind, as well as the natural frequencies of a free-fixed non-Goupillaud-type layered strip.

Published by Elsevier B.V.

1. Introduction

The study of natural vibrations in elastic media include the study of resonance, as resonance can enhance the performance of many sensors and devices, yet can devastate structures subjected to sustained temporally-periodic loading. Despite the long history of developments in the field, exact solutions for the resonance response of multilayered elastic media have been primarily limited to analyses involving only a few layers.

* Corresponding author. Tel.: +1 410 306 0863; fax: +1 410 306 0676.
E-mail address: george.a.gazonas.civ@mail.mil (G.A. Gazonas).

0165-2125/$ – see front matter. Published by Elsevier B.V.
doi:10.1016/j.wavemoti.2011.08.002

A number of works establish the natural modes of vibration in multilayered media [1,2], and analogous problems for n-segmented strings [3] and n-strings [4]. Churchill [5] uses Laplace transform methods to derive the transient resonance response of a free-fixed elastic bar, and notes the presence of the product of a temporal term and time-harmonic function in the solution that becomes unbounded at large times. Caviglia and Morro provide closed-form, time-domain expressions for transient waves in a multilayered elastic (possibly anisotropic) medium [6]. They derive the transient resonance response of a single isotropic elastic layer sandwiched between two halfspaces that is subjected to a temporally periodic sawtooth function, and observe that resonance makes the elastic layer acoustically transparent. A similar two-dimensional problem is studied by Kaplunov and Krynkin [7] who examine the influence of layer stiffness and thickness on the resonance vibrations in a symmetrically point-loaded single layer of elastic material enclosed between two half-spaces. Qiang et al. [8] study the natural frequencies of anisotropic multilayers, and illustrate beat phenomena in two and three layer systems using an efficient numerical eigensolution scheme that is based on semi-analytical methods. Exact expressions for the reflection coefficients for a two-dimensional elastic layer overlying an elastic halfspace are obtained by Fokina and Fokin [9], but the transient response of the system at resonance is not analyzed. Graff presents a general method [10] to determine the natural frequencies of composite rods for power ultrasonic applications with a specific solution for a two-rod system. The method can be extended to multilayered systems but the general problem of determining the natural frequencies with specific geometry and material properties can only be solved using numerical methods.

Exact analytical expressions for the transient resonance response of a multilayered elastic medium are derivable, however, if we specialize the medium to be of Goupillaud-type [11,12]. The Goupillaud specialization is often used in geophysical applications to model wave propagation in inhomogeneous media [13]. Additional simplifications due to transformation of the spatial variable to the travel-time variable have been particularly useful in this work [14,15]. The transformation has simplified the initial-boundary value problem as well as the frequency equation, allowing us to derive analytical expressions for the natural frequency spectrum in free-fixed Goupillaud-type multilayered media. In addition, the present treatment uses a global matrix method that is attributed to Knopoff [16], rather than the Thomson–Haskell transfer matrix formalism [17,18]. Since the recursion relations for the multilayered medium are written only in terms of the stresses, only half the number of equations are required relative to those in classical global matrix methods [16].

Finally, Bube and Burridge [19] treat the inverse problem of finding the coefficients of a first order 2×2 hyperbolic system related to reflection seismology. In order to numerically solve the continuous initial-boundary-value problem, several difference schemes are applied, as discretizations to the corresponding differential equations. The difference scheme IVp, given in equation (3.1.11) pg. 517 of [19], appears to match the recursive relations for the stress values given in Section 2. The recursion relations and trigonometric stress solutions are shown to be exact, for discretely layered media of Goupillaud-type. The stress solutions that are derived herein using z-transform methods, are used to determine the resonance response for the discrete model, and subsequently extended to the continuous model.

The remainder of the paper is organized as follows. In Section 2, we derive stress solutions at resonance and non-resonance frequencies for a Goupillaud-type elastic medium subjected to the given boundary conditions. This is accomplished by generalizing the global system of recursion relations previously derived in [20] and using z-transform methods. The determinant of the global system matrix $|\mathbf{A_m}|$ is a palindromic polynomial with real coefficients. We prove that the zeros of $|\mathbf{A_m}|$ are distinct, complex conjugate, and lie on the unit circle for $1 \leq m \leq 5$ and for certain classes of multilayered designs identified by tridiagonal Toeplitz matrices. The zeros of the determinant allow us to identify the resonance frequency spectrum for the discrete model. The resonance results derived for the discrete model in Section 2 are extended to the continuous model in Section 3, using a linear transformation between the frequencies of the discrete and continuous forcing function. As a result, we are able to analytically describe the natural frequency spectrum of a free-fixed Goupillaud-type strip. An alternative derivation for the natural frequency spectrum is also provided in Section 3 through a generalization of Graff's method [10]. Common to the analysis in Sections 2 and 3 is the transformation and simplification of the initial boundary value problem which replaces the spatial variable x with the travel-time variable ξ. Various applications and interpretations are discussed in Section 4. Section 5 summarizes the results, while miscellaneous references and derivations are included in the Appendices.

2. Discrete forcing function and resonance frequencies

2.1. Description of the discrete model

A finite strip made of m-layers of homogeneous elastic materials is considered, where the density and elastic modulus of the material occupying the ith layer are represented by ρ_i and E_i respectively, for $i = 1, \ldots, m$. We relate to the ith layer, the wave speed $c_i = (E_i/\rho_i)^{1/2}$ and the characteristic impedance $\rho_i \cdot c_i$, for $i = 1, \ldots, m$. The material properties and the wave speed are piecewise constant functions, taking constant values in each layer. The impedance ratio between layers i and $i+1$ is represented by $\alpha_i = \frac{c_i \rho_i}{c_{i+1}\rho_{i+1}} = \frac{\sqrt{E_i \rho_i}}{\sqrt{E_{i+1}\rho_{i+1}}}$, for $i = 1, \ldots, m-1$, while the transit time through the strip is denoted by τ. The m-layered strip is of Goupillaud-type, which means equal wave travel time of $\frac{\tau}{m}$ for each layer. The strip is subjected to zero initial conditions, a discrete loading function $f(n)$, at one end, with $n \geq 0$ and step $\frac{2\tau}{m}$, and held fixed at the other end,

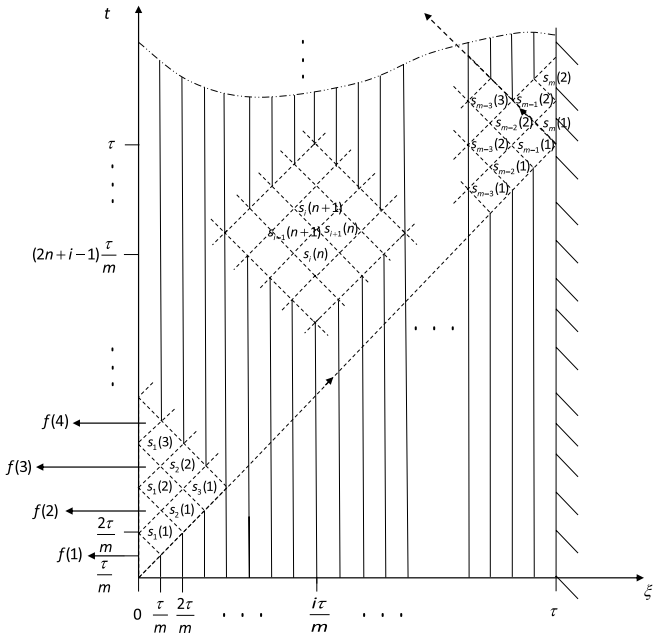

Fig. 1. Lagrangian diagram for an elastic strip made of m-layers of equal wave travel time.

see Fig. 1. As a result, our initial-boundary value problem is

$$\begin{cases} \dfrac{\partial^2 u(x,t)}{\partial t^2} = c_i^2 \dfrac{\partial^2 u(x,t)}{\partial x^2}, & \text{for } x_{i-1} < x < x_i \ \ i = 1, \ldots, m, \ \text{and} \ \ t > 0, \\ \sigma(0,t) = E_1 \dfrac{\partial u}{\partial x}(0,t) = f(n), & \text{for } \ (n-1)\dfrac{2\tau}{m} < t < n\dfrac{2\tau}{m}, \ n \geq 1, \ \text{and} \ \ t > 0, \\ u(L,t) = 0, \\ u(x,0) = \dfrac{\partial u}{\partial x}(x,0) = 0. \end{cases} \tag{1}$$

The functions $u(x,t)$ and $\sigma(x,t)$ represent the displacement and stress respectively. The layer interface between the ith and the $(i+1)$th layer is located at x_i for $i = 1, \ldots, m-1$; $x_0 = 0$ and $x_m = L$, where L represents the length of the strip. By replacing the spatial variable x with the travel-time variable ξ, defined in [14,15] and below,[1]

$$\xi = \xi(x) = \int_0^x \frac{\mathrm{d}s}{c(s)}, \tag{2}$$

it follows that $\frac{\mathrm{d}\xi}{\mathrm{d}x} = c(x)$ and our initial-boundary value problem (1) becomes

$$\begin{cases} \dfrac{\partial^2 u(\xi,t)}{\partial t^2} = \dfrac{\partial^2 u(\xi,t)}{\partial \xi^2}, & \text{for } \dfrac{(i-1)\tau}{m} < \xi < \dfrac{i\tau}{m}, \ \ i = 1, \ldots, m, \ \text{and} \ \ t > 0, \\ \sigma(0,t) = \dfrac{E_1}{c_1}\dfrac{\partial u}{\partial \xi}(0,t) = \tilde{E}_1 \dfrac{\partial u}{\partial \xi}(0,t) = f(n), & \text{for } \ (n-1)\dfrac{2\tau}{m} < t < n\dfrac{2\tau}{m}, \ n \geq 1, \ \text{and} \ \ t > 0, \\ u(\tau,t) = 0, \\ u(\xi,0) = \dfrac{\partial u}{\partial \xi}(\xi,0) = 0. \end{cases} \tag{3}$$

Due to the transformation of variables (2), problem (1) is simplified to a Goupillaud-type strip with length equal to the transit time τ through the strip, layer lengths equal to $\frac{\tau}{m}$, wave travel time equal to $\frac{\tau}{m}$ for each layer in either direction, and wave speed of unity in each layer, as seen from the first equation in (3). The material properties of the ith layer are represented by E_i and ρ_i for the physical case (1) and $\tilde{\rho}_i$ and $\tilde{E}_i$ for the simplified case (3). Having $\tilde{\rho}_i = \tilde{E}_i = \frac{E_i}{c_i} = \sqrt{E_i \rho_i}$, it follows that the impedance ratios $\alpha_i = \frac{\sqrt{E_i\rho_i}}{\sqrt{E_{i+1}\rho_{i+1}}} = \frac{\sqrt{\tilde{E}_i\tilde{\rho}_i}}{\sqrt{\tilde{E}_{i+1}\tilde{\rho}_{i+1}}} = \frac{\tilde{E}_i}{\tilde{E}_{i+1}}$ and the stress values $E_1\frac{\partial u}{\partial x} = \frac{E_1}{c_1}\frac{\partial u}{\partial \xi} = \tilde{E}_1\frac{\partial u}{\partial \xi}$, $i = 1, 2, \ldots, m-1$, remain unchanged as a result of the transformation of variables (2). Therefore, in all our derivations

[1] Here, $c \equiv c(s)$ is the piecewise constant wave speed function taking a constant value in each layer.

of the stress solutions, we focus on the simplified case (3). As shown in Fig. 1, the original coordinates of the boundary and layer interfaces $x_0 = 0 < x_1 < x_2 \cdots < x_i < \cdots < x_m = L$ are replaced by the new coordinates $\xi_0 = 0 < \xi_1 = \frac{\tau}{m} < \xi_2 = \frac{2\tau}{m} < \cdots < \xi_i = \frac{i\tau}{m} < \cdots \xi_m = \tau$ for $i = 1, 2, \ldots, m$. The time variable t is represented on the vertical axis and $\frac{\tau}{m}$ represents the (equal) wave travel time for each layer of the m-layered strip in either direction. The inner vertical solid lines represent the layer interfaces.

Due to the continuity of stress and displacement at each layer interface, the stress values are constant in each square and half-diamond subregion. The unknown stress values are represented by $s_i(n)$ for $i = 1, 2, \ldots, m$ and $n \geq 1$. In a given layer i, the stress values alternate (interlace) between $s_{i-1}(n)$ and $s_i(n)$ for $i = 1, 2, \ldots, m$, $s_0(n) = f(n)$, and $n = 1, 2, \ldots$. From the superposition of the transmitted and reflected waves at the layer interfaces and boundary, a system of coupled first order difference equations for the stress terms was developed in [20] for the special case of a Heaviside step in stress loading $f(n) = p = \textit{constant}$ and $n \geq 0$. The present work generalizes this system by replacing the Heaviside step in stress loading with an arbitrary discrete loading function $f(n)$, $n \geq 0$, as shown below

$$\begin{cases} s_1(n+1) = -s_1(n) + \dfrac{2\alpha_1}{1+\alpha_1} s_2(n) + \dfrac{2}{1+\alpha_1} f(n+1), \\ s_i(n+1) = -s_i(n) + \dfrac{2\alpha_i}{1+\alpha_i} s_{i+1}(n) + \dfrac{2}{1+\alpha_i} s_{i-1}(n+1), \quad \text{for } i = 2, \ldots, m-1, \\ s_m(n+1) = -s_m(n) + 2s_{m-1}(n+1), \end{cases} \tag{4}$$

subject to the zero-stress initial conditions $s_i(0) = 0$ for $1 \leq i \leq m$. Here $n \geq 0$ is a suitable time index and $s_i(n)$ represent the stress terms for $1 \leq i \leq m$ (see Fig. 1). The discrete function $f(n)$, $n \geq 0$, represents the stress loading applied at $\xi = 0$. Notice that by applying the limiting condition $\alpha_i \to 0$ to the recursive relation $s_i(n+1) = -s_i(n) + \frac{2\alpha_i}{1+\alpha_i} s_{i+1}(n) + \frac{2}{1+\alpha_i} s_{i-1}(n+1)$ for $i = m$, we recover the last equation in (4), corresponding to the fixed end. A similar system of difference equations may be obtained for other initial and boundary conditions.

System (4) can then be solved using z-transform methods.[2] As a result, the z-transform of (4) is expressed as

$$\begin{cases} zS_1(z) = -S_1(z) + \dfrac{2\alpha_1}{1+\alpha_1} S_2(z) + \dfrac{2}{1+\alpha_1} z(F(z) - f(0)), \\ zS_i(z) = -S_i(z) + \dfrac{2\alpha_i}{1+\alpha_i} S_{i+1}(z) + \dfrac{2}{1+\alpha_i} zS_{i-1}(z), \quad \text{for } i = 2, \ldots, m-1, \\ zS_m(z) = -S_m(z) + 2zS_{m-1}(z). \end{cases} \tag{5}$$

After reorganizing the terms in (5), the linear system is written in matrix-vector form as

$$\mathbf{A_m}\vec{\mathbf{x}}_\mathbf{m} = \vec{\mathbf{b}}_\mathbf{m}, \tag{6}$$

where $\mathbf{A_m}$ is a tridiagonal matrix given as

$$\mathbf{A_m} = \begin{bmatrix} z+1 & -\eta_1\alpha_1 & 0 & \cdots & 0 & 0 & 0 & 0 \\ -\eta_2 z & z+1 & -\eta_2\alpha_2 & 0 & \cdots & 0 & 0 & 0 \\ 0 & -\eta_3 z & z+1 & -\eta_3\alpha_3 & 0 & \cdots & 0 & 0 \\ \ddots & \ddots & \ddots & & \ddots & \ddots & \ddots & \\ 0 & 0 & 0 & \cdots & 0 & -\eta_{m-1}z & z+1 & -\eta_{m-1}\alpha_{m-1} \\ 0 & 0 & 0 & \cdots & 0 & 0 & -\eta_m z & z+1 \end{bmatrix}_{m\times m}, \tag{7}$$

while

$$\vec{\mathbf{x}}_\mathbf{m} = \begin{bmatrix} S_1(z) \\ S_2(z) \\ \vdots \\ S_m(z) \end{bmatrix}_{m\times 1}, \qquad \vec{\mathbf{b}}_\mathbf{m} = \begin{bmatrix} \eta_1 z(F(z) - f(0)) \\ 0 \\ \vdots \\ 0 \end{bmatrix}_{m\times 1},$$

$$\eta_i = \frac{2}{1+\alpha_i} \quad \text{for } i = 1, \ldots, m-1,\ \eta_m = 2.$$

Due to the sparseness of $\vec{\mathbf{b}}_\mathbf{m}$, the solution of the linear system (6) is

$$\vec{\mathbf{x}}_\mathbf{m} = \mathbf{A}_\mathbf{m}^{-1}\vec{\mathbf{b}}_\mathbf{m} = \frac{\eta_1 z(F(z) - f(0))}{|\mathbf{A_m}|} \begin{bmatrix} (-1)^{1+1}|\mathbf{A_{1,1}}| \\ (-1)^{1+2}|\mathbf{A_{1,2}}| \\ \vdots \\ (-1)^{1+m}|\mathbf{A_{1,m}}| \end{bmatrix}. \tag{8}$$

[2] The definition for the z-transform of $g(n)$, $n \geq 0$, is $Z(g(n)) = G(z) = \sum_{n=0}^{\infty} g(n) z^{-n}$ for $|z| > R$ in the complex plane (see [21]).

Here $|\mathbf{A_m}|$ and $|\mathbf{A_{1,i}}|$ are the determinants of $\mathbf{A_m}$ and its minor $\mathbf{A_{1,i}}$, for $i = 1, \ldots, m$. The following recursive relation holds:

$$|\mathbf{A_m}| = (z+1)|\mathbf{A_{m-1}}| - \eta_1\eta_2\alpha_1 z|\mathbf{A_{m-2}}|, \tag{9}$$

where $\mathbf{A_m}$ corresponds to the m-layered strip with impedance ratios $\alpha_1, \alpha_2, \ldots, \alpha_{m-1}$; $\mathbf{A_{m-1}}$ corresponds to the remaining $(m-1)$-layered strip with impedance ratios $\alpha_2, \alpha_3, \ldots, \alpha_{m-1}$, obtained after the removal of the first layer from the m-layered strip; $\mathbf{A_{m-2}}$ corresponds to the remaining $(m-2)$-layered strip with impedance ratios $\alpha_3, \ldots, \alpha_{m-1}$, obtained after the removal of the first two layers from the m-layered strip. One can derive by induction that the determinant $|\mathbf{A_m}|$ is a palindromic polynomial with real coefficients; i.e. the coefficients in front of z^{m-j} and z^j are real and equal to each-other for $j = 0, \ldots, m$ and $m \geq 1$. The complex roots of a polynomial with real coefficients occur in conjugate pairs, and since the coefficients are palindromic, then the roots also occur in inverse pairs. Since the inverse pairing is not necessarily the same as the conjugate pairing, if a root's inverse is not its complex conjugate, then it must be one of a set of four related roots that satisfy a palindromic quartic with real coefficients. As a result, each palindromic polynomial of even degree is expected to factor into quadratic and quartic palindromes with real coefficients. In Section 2.2 below, the quadratic and quartic factors of $|\mathbf{A_m}|$ for $1 \leq m \leq 5$, are shown to satisfy the necessary and sufficient conditions for all their roots to be distinct (complex conjugate) on the unit circle. As a result, the determinant $|\mathbf{A_m}|$ can be factored into quadratic palindromes with real coefficients for $1 \leq m \leq 5$, as presented later in (15).

2.2. On the zeros of the determinant $|\mathbf{A_m}|$

The expressions for the determinant $|\mathbf{A_m}|$ using the recursive relation (9) for $1 \leq m \leq 5$ are:

$$\begin{aligned}
&|\mathbf{A_1}| = z+1, \qquad |\mathbf{A_2}| = (z+1)^2 - \eta_2\eta_1\alpha_1 z = z^2 - \frac{2(\chi_1-2)}{\chi_1}z + 1,\\
&|\mathbf{A_3}| = (z+1)\cdot\left[z^2 - \frac{2(\chi_2-2)}{\chi_2}z + 1\right], \qquad |\mathbf{A_4}| = z^4 - \frac{4\Gamma_3}{\chi_3}z^3 + \frac{2(4\Gamma_3-\chi_3+8)}{\chi_3}z^2 - \frac{4\Gamma_3}{\chi_3}z + 1,\\
&|\mathbf{A_5}| = (z+1)\cdot\left[z^4 - \frac{4\Gamma_4}{\chi_4}z^3 + \frac{2(4\Gamma_4-\chi_4+8)}{\chi_4}z^2 - \frac{4\Gamma_4}{\chi_4}z + 1\right].
\end{aligned} \tag{10}$$

The design parameters involved are: $\chi_{m-1} = \prod_{i=1}^{m-1}(1+\alpha_i)$ for $m \geq 2$, $\Gamma_3 = \alpha_1\alpha_3 - 1$, and $\Gamma_4 = \alpha_1\alpha_3\alpha_4 + \alpha_1\alpha_2\alpha_4 + \alpha_1\alpha_4 + \alpha_2\alpha_4 + \alpha_1\alpha_3 - 1$. Next, the necessary and sufficient conditions (I) and (II) are applied to the quadratic and quartic factors of $|\mathbf{A_m}|$ respectively, to prove that all the zeros of $|\mathbf{A_m}|$ in (10) are on the unit circle and distinct for $1 \leq m \leq 5$. As for the linear factor $(z+1)$ which appears for m-odd, the zero $z = -1$ already is on the unit circle and distinct from all the other zeros.

(I) *The zeros of a quadratic factor with real coefficients of the form $z^2 + \mu z + 1$ are distinct (complex conjugate) on the unit circle iff $\mu^2 - 4 < 0$ or equivalently iff $|\mu| < 2$.*

For $m = 2, 3$, we have from (10) that $\mu = \mu_m = -\frac{2(\chi_{m-1}-2)}{\chi_{m-1}}$. Therefore the condition $|\mu| < 2$ becomes equivalent to $\left|\frac{\chi_{m-1}-2}{\chi_{m-1}}\right| < 1$, which is true because $\chi_{m-1} > 1$.

(II) *The zeros of a quartic factor with real coefficients of the form $z^4 + \mu z^3 + \nu z^2 + \mu z + 1$ are distinct (complex conjugate) on the unit circle[3] iff $[\mu^2 - 4\nu + 8 > 0$ and $|\frac{-\mu \pm \sqrt{\mu^2-4\nu+8}}{2}| < 2]$.*

For $m = 4, 5$, we have from (10) that $\mu = \mu_m = -\frac{4\Gamma_{m-1}}{\chi_{m-1}}$ and $\nu = \nu_m = \frac{2(4\Gamma_{m-1}-\chi_{m-1}+8)}{\chi_{m-1}}$.

- The requirement $\mu^2 - 4\nu + 8 > 0$ becomes equivalent to $[(\chi_{m-1}-\Gamma_{m-1})^2 - 4\chi_{m-1}] = [(\Upsilon_{m-1}-2)^2 - 4(1+\Gamma_{m-1})] > 0$, where $\Upsilon_{m-1} = \chi_{m-1} - \Gamma_{m-1}$. The desired inequality follows from the following relations:
  $(\Upsilon_3 - 2)^2 - 4(1+\Gamma_3) > (\alpha_1+\alpha_3)^2 - 4\alpha_1\alpha_3 = (\alpha_1-\alpha_3)^2 \geq 0$ for $m = 4$, and $(\Upsilon_4-2)^2 - 4(1+\Gamma_4) > (\alpha_1+\alpha_2+\alpha_1\alpha_2+\alpha_3+\alpha_4+\alpha_3\alpha_4)^2 - 4(1+\Gamma_4) > (-\alpha_1-\alpha_2-\alpha_1\alpha_2+\alpha_3+\alpha_4+\alpha_3\alpha_4)^2 \geq 0$ for $m = 5$.
- The requirement $\left|\frac{-\mu \pm \sqrt{\mu^2-4\nu+8}}{2}\right| < 2$ is equivalent to $\left|\frac{\Gamma_{m-1} \pm \sqrt{(\chi_{m-1}-\Gamma_{m-1})^2 - 4\chi_{m-1}}}{\chi_{m-1}}\right| < 1$, which is true because $\chi_{m-1} > 1 > 0$ and $\Gamma_{m-1} + 1 > 0$ for $m = 4, 5$. As seen later in (A.5)–(A.7), the two requirements in (II) guarantee real cosine values.

For the general m-layer case, our preliminary results with tridiagonal Toeplitz matrices, show that we can find designs with any number of layers for which all the zeros of $|\mathbf{A_m}|$ are distinct, have no multiples, and are on the unit circle. Indeed,

[3] This criterion is derived after dividing the quartic polynomial by z^2 and then applying the transformation $y = z + \frac{1}{z}$.

using standard techniques, the symmetric matrix $\mathbf{G_m}$ can be formed such that $|\mathbf{A_m}| = |\mathbf{G_m}|$,

$$\mathbf{G_m} = \begin{bmatrix} z+1 & \sqrt{z\zeta_1} & 0 & \cdots & 0 & 0 & 0 & 0 \\ \sqrt{z\zeta_1} & z+1 & \sqrt{z\zeta_2} & 0 & \cdots & 0 & 0 & 0 \\ 0 & \sqrt{z\zeta_2} & z+1 & \sqrt{z\zeta_3} & 0 & \cdots & 0 & 0 \\ \ddots & \ddots & \ddots & & \ddots & \ddots & \ddots & \\ 0 & 0 & 0 & \cdots & 0 & \sqrt{z\zeta_{m-2}} & z+1 & \sqrt{z\zeta_{m-1}} \\ 0 & 0 & 0 & \cdots & 0 & 0 & \sqrt{z\zeta_{m-1}} & z+1 \end{bmatrix}_{m\times m} \tag{11}$$

with $\zeta_i = \alpha_i\eta_i\eta_{i+1}$ for $i = 1, 2, \ldots, m-1$. As before, $\eta_i = \frac{2}{1+\alpha_i}$ for $i = 1, \ldots, m-1$ and $\eta_m = 2$. If $\mathbf{G_m}$ has constant off-diagonal terms, i.e., $\sqrt{z\zeta_1} = \sqrt{z\zeta_2} = \cdots \sqrt{z\zeta_{m-1}} = \sqrt{z\zeta}$ or equivalently $\zeta = \alpha_i\eta_i\eta_{i+1}$ for $i = 1, 2, \ldots, m-1$. Then $\mathbf{G_m}$ is a tridiagonal Toeplitz matrix with palindromic determinant $|\mathbf{G_m}|$ which can be written as [22],

$$|\mathbf{G_m}| = \prod_{k=1}^{m} \left(z + 1 - 2\sqrt{z\zeta}\, g(k,m) \right), \tag{12}$$

or equivalently,

$$|\mathbf{G_m}| = \begin{cases} \displaystyle\prod_{k=1}^{\lfloor \frac{m}{2} \rfloor} \left[z^2 + 2z\left(1 - 2\zeta g^2(k,m)\right) + 1 \right] & \text{for } m \text{ even}, \\ \displaystyle (z+1) \prod_{k=1}^{\lfloor \frac{m}{2} \rfloor} \left[z^2 + 2z\left(1 - 2\zeta g^2(k,m)\right) + 1 \right] & \text{for } m \text{ odd}, \end{cases} \tag{13}$$

where $g(k,m) = \cos\left(\frac{k\pi}{m+1}\right)$. For $0 < \zeta < 1$, the zeros of the quadratic factors in (13),

$$z_k = 2\zeta g^2(k,m) - 1 \pm 2i\sqrt{\zeta g^2(k,m)\left(1 - \zeta g^2(k,m)\right)}, \tag{14}$$

are distinct, complex conjugate, and on the unit circle, with $|z_k|^2 = z_k\bar{z}_k = 1$ and $\arg(z_k) = \theta_k$, for all $1 \le k \le \lfloor \frac{m}{2} \rfloor$. For these ζ-values, the representation in (13) becomes consistent with (15). In our numerical experiments displayed later in Fig. 5a, b, for a given value of ζ, $0 < \zeta < 1$, the impedance ratios are derived from the recursive relations: $\alpha_{m-1} = \frac{\zeta}{4-\zeta}$ and $\alpha_i = -1 + \frac{4}{4-\zeta-\zeta\alpha_{i+1}}$ for $i = 1, \ldots, m-2$. Other tridiagonal [23,24] or k-Toeplitz [25,26] matrices, which have analytical expressions for their determinants like that given by (12), may also be studied in an attempt to generalize the class of media for which the roots of $|\mathbf{G_m}| = 0$ are distinct and on the unit circle for arbitrary m.

In this paper, we only consider m-layered designs for which all the zeros of $|\mathbf{A_m}|$ are distinct, have no multiples, and are on the unit circle. Based on the results above, this class of designs is not empty. For $z_k = e^{\mathbb{1}\theta_k} = \cos\theta_k + \mathbb{1}\sin\theta_k$, we have that $z_k^{-1} = \bar{z}_k = e^{\mathbb{1}\theta_k} = \cos\theta_k - \mathbb{1}\sin\theta_k$ and $(z - e^{\mathbb{1}\theta_k})(z - e^{-\mathbb{1}\theta_k}) = z^2 - 2z\cos\theta_k + 1$. As a result, a newly factored representation of $|\mathbf{A_m}|$ is obtained, with palindromic quadratics with real coefficients involving the cosines of the angles $\theta_1, \theta_2, \ldots, \theta_{\lfloor \frac{m}{2} \rfloor}$ and linear factor $(z+1)$ for m-odd,

$$|\mathbf{A_m}| = \begin{cases} \displaystyle\prod_{k=1}^{\lfloor \frac{m}{2} \rfloor} [z^2 - 2z\cos\theta_k + 1] & \text{for } m \text{ even}, \\ \displaystyle (z+1) \prod_{k=1}^{\lfloor \frac{m}{2} \rfloor} [z^2 - 2z\cos\theta_k + 1] & \text{for } m \text{ odd}. \end{cases} \tag{15}$$

2.3. General formulas for the stress and resonance frequencies

Based on the factorization of the determinant $|\mathbf{A_m}|$ given in (15), for any m-layered design, if there are m distinct roots on the unit circle, there are m distinct angles. The $\lfloor \frac{m}{2} \rfloor$ essential angles $0 < \theta_k < \pi$ for $k = 1, \ldots, \lfloor \frac{m}{2} \rfloor$ were known in [20] as the base angles. The equations for the angles $\theta_0 = \pi$ and $\{\theta_k\}_{k=1}^{\lfloor \frac{m}{2} \rfloor}$ in terms of the design parameters (combinations of the impedance ratios) for up to five layers are derived in [20]. Since the degree of $|\mathbf{A_m}|$ is m and the degree of $|\mathbf{A_{1,i}}|$ is $m-1$, for $i = 1, 2, \ldots, m$, the substitution of (15) into (8), results in the following expansion of the components $\vec{\mathbf{x}}_\mathbf{m}(i)$ of $\vec{\mathbf{x}}_\mathbf{m}$ into partial fractions:

$$\vec{\mathbf{x}}_{\mathbf{m}}(i) = z(F(z)-f(0))\left[\frac{\eta_1(-1)^i|\mathbf{A}_{\mathbf{1,i}}|}{|\mathbf{A}_{\mathbf{m}}|}\right]$$
$$= z(F(z)-f(0))\left[\frac{b_{i,0}}{z+1}+\sum_{k=1}^{\lfloor\frac{m}{2}\rfloor}\frac{a^*_{i,k}z+b^*_{i,k}}{z^2-2z\cos\theta_k+1}\right] = (F(z)-f(0))\left[\frac{b_{i,0}z}{z+1}+\sum_{k=1}^{\lfloor\frac{m}{2}\rfloor}\frac{a^*_{i,k}z^2+b^*_{i,k}z}{z^2-2z\cos\theta_k+1}\right], \quad (16)$$

where $b_{i,0}=0$ for m even and $i=1,2,\ldots,m$. After applying the inverse z-transform to (16), a general representation for the stress terms in (4) is obtained,

$$s_i(n) = Z^{-1}(\vec{\mathbf{x}}_{\mathbf{m}}(i)) = f(n) * \left[b_{i,0}(-1)^n+\sum_{k=1}^{\lfloor\frac{m}{2}\rfloor}a_{i,k}\cos(n\theta_k)+b_{i,k}\sin(n\theta_k)\right]$$
$$-f(0)\cdot\left[b_{i,0}(-1)^n+\sum_{k=1}^{\lfloor\frac{m}{2}\rfloor}a_{i,k}\cos(n\theta_k)+b_{i,k}\sin(n\theta_k)\right], \quad (17)$$

for the following choices of the coefficients,

$$a_{i,k}=a^*_{i,k}, \qquad b_{i,k}=\frac{a^*_{i,k}\cos\theta_k+b^*_{i,k}}{\sin\theta_k} \quad \text{for } k=1,\ldots,\left\lfloor\frac{m}{2}\right\rfloor,$$

for $i=1,2,\ldots,m$ and $n\geq 0$. The operation $*$ means convolution. The stress representation previously derived in [20] can now be recovered for the special choice of loading $f(n)=p$ for $n\geq 0$. The stress representation in (17) involves sums of sines and cosines of multiples of angles, which relate to the Chebyshev polynomials of the first and second kind. For the choice of $f(n)=\sin(n\tilde{\omega})$, $n\geq 0$, after substituting $f(0)=0$ and $F(z)=Z(f(n))=Z(\sin(n\tilde{\omega}))=\frac{z\sin(\tilde{\omega})}{(z^2-2z\cos\tilde{\omega}+1)}$ into (16), and then applying the inverse z-transform we get

$$s_i(n)=b_{i,0}Z^{-1}\left[\frac{z^2\sin(\tilde{\omega})}{(z^2-2z\cos\tilde{\omega}+1)(z+1)}\right]+\sum_{k=1}^{\lfloor\frac{m}{2}\rfloor}Z^{-1}\left[\frac{z\sin(\tilde{\omega})\cdot(a^*_{i,k}z^2+b^*_{i,k}z)}{(z^2-2z\cos\theta_k+1)(z^2-2z\cos\tilde{\omega}+1)}\right]. \quad (18)$$

In the subsections that follow, the inverse z-transform is applied to the expressions in (18) to derive the stress formulas at resonance and non-resonance frequencies; the results are verified with numerical experiments. Based on these results, we prove that the resonance frequency spectrum for the discrete model consists of all the positive angles coterminal with $\theta_0=\pi$ or $\{\pm\theta_k\}_{k=1}^{\lfloor\frac{m}{2}\rfloor}$, as shown below

$$\begin{cases}\tilde{\omega}_{l_0}=\theta_0+2l_0\pi=(2l_0+1)\pi & (\text{for } m \text{ odd only}),\\ \tilde{\omega}_{l_1,k}=\theta_k+2l_1\pi, & l_0,l_1,l_2=0,1,2,\ldots,\\ \tilde{\omega}_{l_2,k}=-\theta_k+2(l_2+1)\pi, & k=1,\ldots,\left\lfloor\frac{m}{2}\right\rfloor\end{cases} \quad (19)$$

or equivalently,

$$\begin{cases}\cos\tilde{\omega}=-1 & (\text{for } m \text{ odd only}),\\ \cos\tilde{\omega}=\cos\theta_k & \text{for } k=1,\ldots,\left\lfloor\frac{m}{2}\right\rfloor.\end{cases} \quad (20)$$

The fact that the θ-angles depend only on (certain combinations of) the impedance ratios implies that the resonance frequencies for the discrete model in (19) depend on the same combinations of the impedance ratios and no other parameters.

2.4. Stress solutions at non-resonance frequencies

Here we show that the values of the driving frequency $\tilde{\omega}$ that satisfy $\cos\tilde{\omega}\neq\cos\theta_0=-1$ (for m odd), and $\cos\tilde{\omega}\neq\cos\theta_k$ for all $k=1,\ldots,\lfloor\frac{m}{2}\rfloor$, represent non-resonance frequency values. In the set of real numbers, this set of frequency values is the complement of the set of values identified in (20). Indeed, applying the partial fraction expansion to (18), we derive the following stress solutions,

$$s_i(n) = -\frac{b_{i,0}\sin\tilde{\omega}}{2(1+\cos\tilde{\omega})}(-1)^n+\left[\frac{b_{i,0}\sin\tilde{\omega}}{2(1+\cos\tilde{\omega})}+\sum_{k=1}^{\lfloor\frac{m}{2}\rfloor}A_{i,k}\right]\cos(n\tilde{\omega})$$
$$+\left[\frac{b_{i,0}}{2}+\sum_{k=1}^{\lfloor\frac{m}{2}\rfloor}B_{i,k}\right]\sin(n\tilde{\omega})+\sum_{k=1}^{\lfloor\frac{m}{2}\rfloor}C_{i,k}\cos(n\theta_k)+\sum_{k=1}^{\lfloor\frac{m}{2}\rfloor}D_{i,k}\sin(n\theta_k), \quad (21)$$

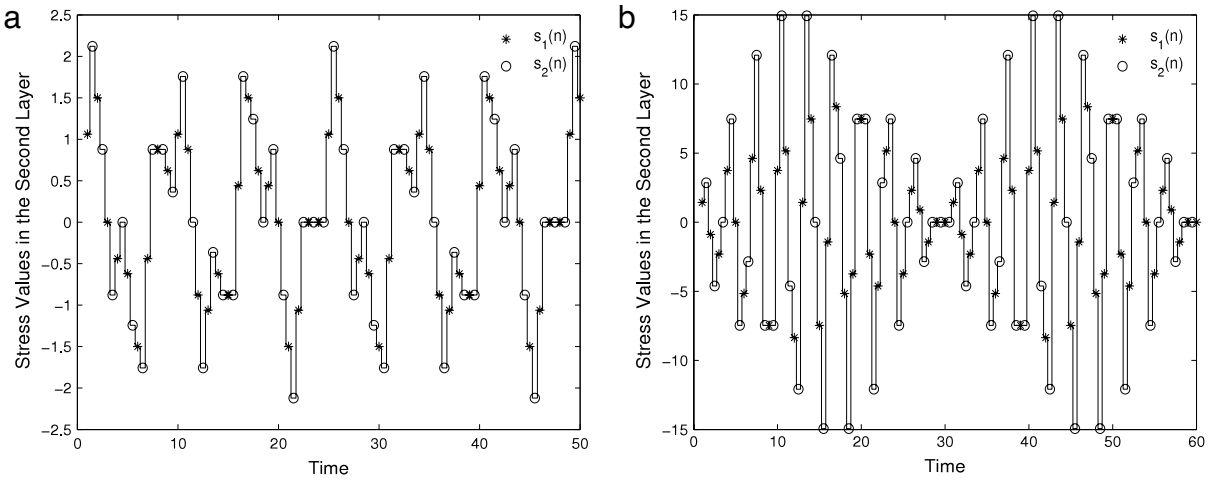

Fig. 2. Stress time history for a two-layered Goupillaud-type strip in the middle of the second layer located at $\xi = 3/4$. Impedance ratio $\alpha_1 = 1/3$, angle $\theta_1 = 2\pi/3$, $\tau = 1$, and loading $f(n) = \sin(n\tilde{\omega})$ at $\xi = 0$. (a) $\tilde{\omega} = \pi/4$. (b) $\tilde{\omega} = 0.9 \cdot \theta_1 = 0.6\pi$.

where

$$A_{i,k} = -C_{i,k} = \frac{a^*_{i,k} \sin\tilde{\omega}}{2(\cos\tilde{\omega} - \cos\theta_k)}, \qquad B_{i,k} = \frac{a^*_{i,k}\cos\tilde{\omega} + b^*_{i,k}}{2(\cos\tilde{\omega} - \cos\theta_k)}, \qquad D_{i,k} = -\frac{(a^*_{i,k}\cos\theta_k + b^*_{i,k})\sin\tilde{\omega}}{2\sin\theta_k(\cos\tilde{\omega} - \cos\theta_k)}. \tag{22}$$

As before, $b_{i,0} = 0$ when the number of layers m is even. For a given value of $\tilde{\omega}$, the stress solutions in (21), including all the coefficients and angles θ_k for $k = 1, \ldots, \lfloor \frac{m}{2} \rfloor$, can be also expressed in terms of the impedance ratios only (see (6)–(8)). Illustrations of the bounded stress solutions at non-resonance frequencies appear in Fig. 2. As depicted in the plots in Fig. 2, when positioned in the middle of the second layer, the time interval at which $s_i(n)$ is reached is $\frac{4n+2i-3}{4} < t < \frac{4n+2i-1}{4}$ for $n \geq 1$ and $i = 1, 2$ (see Fig. 1). Beat phenomena are clearly visible in 2b, as the driving frequency approaches a resonance frequency.

2.5. Stress solutions at resonance frequencies

The stress solutions in (21) suggest that the driving frequencies $\tilde{\omega}$ identified in (20) are resonance frequencies. Here we confirm this by deriving the stress solutions at these expected resonance frequencies, demonstrating that such solutions grow without bound over time while oscillating.

Case I. $\cos(\tilde{\omega}) = -1 = \cos\theta_0$ (for m odd only).

The fact that $\cos(\tilde{\omega}) = -1$ or equivalently that $\tilde{\omega}$ takes values $\tilde{\omega}_{l_0} = (2l_0 + 1)\pi$ for $l_0 = 0, 1, 2, \ldots$, implies that $f(n) = \sin(n\tilde{\omega}) = \sin(n\pi) = 0$ for all $n \geq 0$. As a result, due to the zero input in loading, we will not be able to detect resonance, as concluded by (17). By choosing $f(n) = \cos(n\tilde{\omega}) = \cos(n\pi)$ we overcome this obstacle. Based on (16)–(17), we expect any unbounded stress terms to come from

$$F(z) \cdot \left[\frac{b_{i,0}z}{z+1} + \sum_{k=1}^{\lfloor \frac{m}{2} \rfloor} \frac{a^*_{i,k}z^2 + b^*_{i,k}z}{z^2 - 2z\cos\theta_k + 1} \right] = \frac{z}{z+1} \cdot \left[\frac{b_{i,0}z}{z+1} + \sum_{k=1}^{\lfloor \frac{m}{2} \rfloor} \frac{a^*_{i,k}z^2 + b^*_{i,k}z}{z^2 - 2z\cos\theta_k + 1} \right], \tag{23}$$

after the inverse z-transform is applied. We conclude that the only term in (23) that generates unbounded stress values is $\frac{b_{i,0}z^2}{(z+1)^2}$ for $b_{i,0} \neq 0$, due to the fact that

$$Z^{-1}\left[\frac{b_{i,0}z^2}{(z+1)^2} \right] = b_{i,0} \cdot W_n(-1) = b_{i,0}(-1)^n(n+1). \tag{24}$$

Here $W_n(y)$ represents the Chebyshev polynomial of the second kind evaluated at $y = -1$. Notice that the resonance frequency spectrum $\tilde{\omega}_{l_0} = (2l_0 + 1)\pi$ for $l_0 = 0, 1, 2, \ldots$, *is universal for all the designs with an odd number of layers and it is independent of any design parameters*. This is illustrated in Fig. 3 for the seven- and eleven-layer case.

Case II.a. $\cos\tilde{\omega} = \cos\theta_{k^*}$ and $\sin\tilde{\omega} = \sin\theta_{k^*}$.

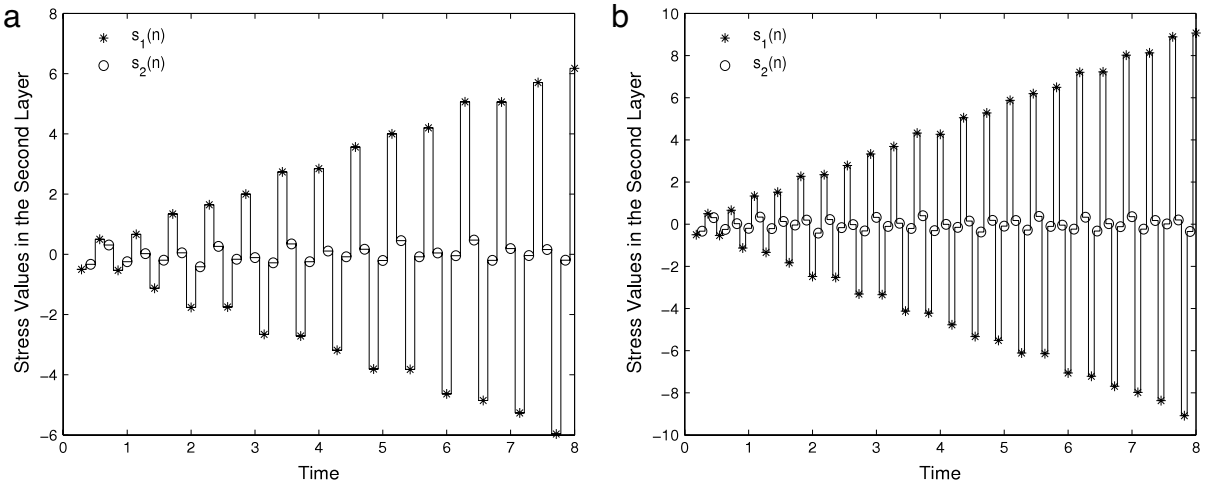

Fig. 3. Stress time history for a multilayered strip with $\tau = 1$ and impedance ratios $\alpha_1 = 3, \alpha_2 = 2, \alpha_3 = 1.5, \alpha_4 = 2.2, \alpha_5 = 0.3, \alpha_6 = 1.7, \alpha_7 = 1.4, \alpha_8 = 3.1, \alpha_9 = 0.8, \alpha_{10} = 4$ as applicable; loading $f(n) = \cos(n\tilde{\omega})$ is applied at $\xi = 0$ for $\tilde{\omega} = \pi$. (a) The middle of the second layer of a seven-layered strip located at $\xi = 3/14$. (b) The middle of the second layer of an eleven-layered strip located at $\xi = 3/22$.

Suitable partial fraction expansions of (18) give the following stress solutions for the frequency spectrum $\tilde{\omega}_{l_1,k^*} = \theta_{k^*} + 2l_1\pi$, $l_1 = 0, 1, 2, \ldots$,

$$\begin{aligned} s_i(n) = & -\frac{b_{i,0}\sin\theta_{k^*}}{2(1+\cos\theta_{k^*})}(-1)^n + \left[\frac{b_{i,0}\sin\theta_{k^*}}{2(1+\cos\theta_{k^*})} + n\tilde{A}_{i,k^*} + \sum_{k=1,k\neq k^*}^{\lfloor\frac{m}{2}\rfloor} A_{i,k}\right]\cos(n\theta_{k^*}) \\ & + \left[\frac{b_{i,0}}{2} + n\tilde{B}_{i,k^*} + \tilde{C}_{i,k^*} + \sum_{k=1,k\neq k^*}^{\lfloor\frac{m}{2}\rfloor} B_{i,k}\right]\sin(n\theta_{k^*}) \\ & + \sum_{k=1,k\neq k^*}^{\lfloor\frac{m}{2}\rfloor} C_{i,k}\cos(n\theta_k) + \sum_{k=1,k\neq k^*}^{\lfloor\frac{m}{2}\rfloor} D_{i,k}\sin(n\theta_k). \end{aligned} \tag{25}$$

Here $A_{i,k}, B_{i,k}, C_{i,k}, D_{i,k}$ are given from (22) for $\tilde{\omega} = \theta_{k^*} + 2l_1\pi, l_1 = 0, 1, 2, \ldots$, while

$$\tilde{A}_{i,k^*} = -\frac{(a^*_{i,k^*}\cos\theta_{k^*} + b^*_{i,k^*})}{2\sin\theta_{k^*}}, \qquad \tilde{B}_{i,k^*} = \frac{a^*_{i,k^*}}{2}, \qquad \tilde{C}_{i,k^*} = \frac{a^*_{i,k^*} + b^*_{i,k^*}\cos\theta_{k^*}}{2\sin^2\theta_{k^*}}. \tag{26}$$

As before, $b_{i,0} = 0$ for m even and $\sin\theta_k \neq 0$ for all $k = 1, \ldots, \lfloor\frac{m}{2}\rfloor$. All the terms in the stress solution (25) are bounded, except $[\tilde{A}_{i,k^*}\cos(n\theta_{k^*}) + \tilde{B}_{i,k^*}\sin(n\theta_{k^*})]\cdot n$, which are multiplied by the time-related linear factor n. This implies that the stress amplitude is expected to grow without bound while oscillating over time, proving resonance.

Case II.b. $\cos\tilde{\omega} = \cos\theta_{k^*}$ and $\sin\tilde{\omega} = -\sin\theta_{k^*} = \sin(-\theta_{k^*})$.

A similar stress representation to (25) can be obtained at the frequency values $\tilde{\omega}_{l_2,k^*} = -\theta_{k^*} + 2(l_2+1)\pi, l_2 = 0, 1, 2, \ldots$, after a sign adjustment for some of the coefficients.

The resonance response in a four- and five-layered elastic strip using the analytical results generated from (25) is illustrated in Fig. 4. This is a demonstration and corroboration of formula (19) in predicting resonance. As illustrated in Fig. 4 for the four-layer case, the base angle $\theta_2 = \cos^{-1}\left(\frac{\Gamma_3 - \sqrt{(\chi_3-\Gamma_3)^2 - 4\chi_3}}{\chi_3}\right)$ represents a resonance frequency. The same is true for the five-layer case and the base angle $\theta_1 = \cos^{-1}\left(\frac{\Gamma_4 + \sqrt{(\chi_4-\Gamma_4)^2 - 4\chi_4}}{\chi_4}\right)$. The relevant design parameters are given by $\chi_{m-1} = \prod_{i=1}^{m-1}(1+\alpha_i)$ for $m = 4, 5$; $\Gamma_3 = \alpha_1\alpha_3 - 1$, and $\Gamma_4 = \alpha_1\alpha_3\alpha_4 + \alpha_1\alpha_2\alpha_4 + \alpha_1\alpha_4 + \alpha_2\alpha_4 + \alpha_1\alpha_3 - 1$ while the impedance ratios are $\alpha_1 = 0.6, \alpha_2 = 1.5, \alpha_3 = 2$, and $\alpha_4 = 1.2$, as applicable.

The resonance response in a twenty two- and thirty nine-layered elastic strip generated from the recursive relations (4) and (13)–(14) is illustrated in Fig. 5.

This is another demonstration and corroboration of formula (19) in predicting resonance. For the twenty two layer case, the base angle corresponding to $k = 11$ and $\zeta = 7/9$ represents a resonance frequency. Similarly for the thirty nine layer case, the base angle obtained for $k = 5$ and $\zeta = 1/2$ represents a resonance frequency. The impedance ratios in both cases are derived from the recursive relations: $\alpha_{m-1} = \frac{\zeta}{4-\zeta}$ and $\alpha_i = -1 + \frac{4}{4-\zeta-\zeta\alpha_{i+1}}$ for $i = 1, \ldots, m-2$.

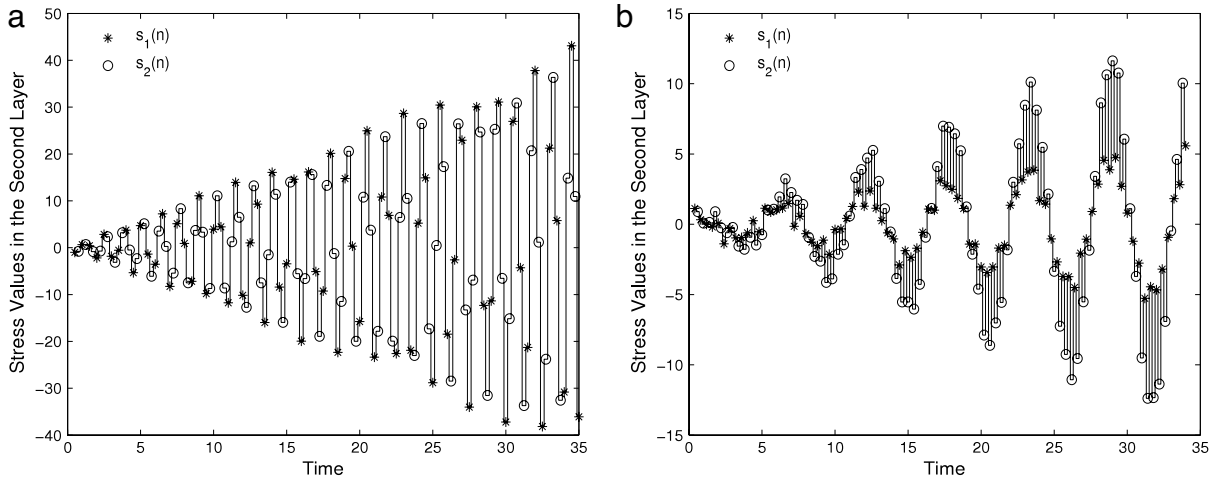

Fig. 4. Stress time history for a multilayered strip with $\tau = 1$ and loading $f(n) = \cos(n\tilde{\omega})$ applied at $\xi = 0$. (a) The middle of the second layer of a four-layered strip located at $\xi = 3/8$, when the driving frequency is $\tilde{\omega} = \theta_2$, $\theta_2 = \cos^{-1}\left(\frac{\Gamma_3 - \sqrt{(\chi_3-\Gamma_3)^2 - 4\chi_3}}{\chi_3}\right)$, $\chi_3 = 12$, $\Gamma_3 = 0.2$. (b) The middle of the second layer of a five-layered strip located at $\xi = 3/10$, when the driving frequency is $\tilde{\omega} = \theta_1$, $\theta_1 = \cos^{-1}\left(\frac{\Gamma_4 + \sqrt{(\chi_4-\Gamma_4)^2 - 4\chi_4}}{\chi_4}\right)$, $\chi_4 = 26.4$, $\Gamma_4 = 5.24$.

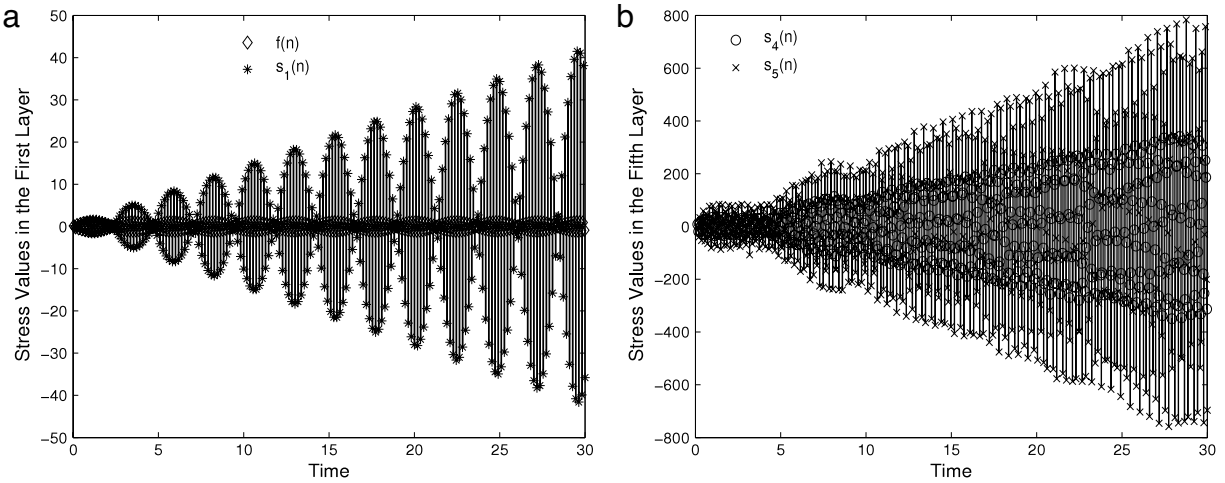

Fig. 5. Stress time history for a multilayered strip with $\tau = 1$ and loading $f(n) = \sin(n\tilde{\omega})$ applied at $\xi = 0$. (a) The middle of the first layer of a twenty two-layered strip when the driving frequency is $\tilde{\omega} = \theta_{11}$, (b) the middle of the fifth layer of a thirty nine-layered strip when the driving frequency is $\tilde{\omega} = \theta_5$.

2.6. Accuracy and precision of the recursive and explicit solutions

Despite the fact that the recursive relations (4) and the explicit formulas (17) are exact, the stress solutions $s_i(n)$, $n \geq 1$, $i = 1, \ldots, m$, calculated from these formulas, are not always exact. Here we show that for a Heaviside stress loading and certain layer properties, the stress solutions represented by terminating decimals are exact, as they do not exhibit roundoff error. In others cases, when the stress solutions are represented by non-terminating decimals, a precision loss is observed. This discussion is particularly important for verification of numerical finite element solutions with "exact" solutions; one should be aware of the loss in precision even in the "exact" solutions [27].

For a free-fixed two-layered strip subjected to a Heaviside loading with layer impedance ratio $\alpha = 3$, the stress in layer 2 is represented by a periodic sequence of 12 rational numbers that can be expressed as terminating decimals $\{\frac{1}{2}, 1, \frac{3}{2}, 2, 2, 2, \frac{3}{2}, 1, \frac{1}{2}, 0, 0, 0, \ldots\}$ (see Fig. 7(b)). Both, the recursive relations (4) and the explicit trigonometric formulas (17) predict this stress sequence exactly for all $n \geq 1$.

Alternatively, for a free-fixed two-layered strip subjected to a Heaviside loading with layer impedance ratio $\alpha = 4$, a loss in precision is observed when a fixed number of significant digits is used in the numerical calculations. The loss of precision

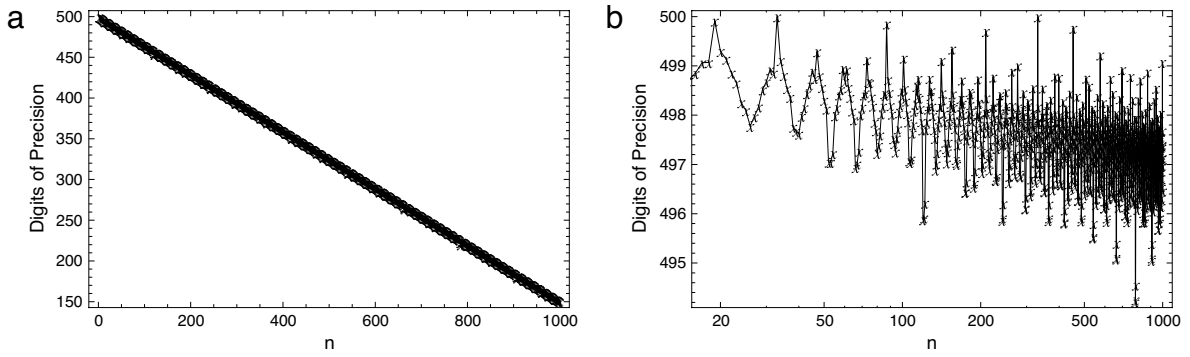

Fig. 6. Precision loss in stress calculations for a two-layered Goupillaud-type strip with $\alpha = 4$, subjected to a Heaviside loading $f(n) = p$. (a) Linear loss in precision obtained from the recursive relations (4), and (b) log-linear loss in precision in the explicit formula (17).

with the recursive relations (4) is due to roundoff error, while the loss of precision with the trigonometric formulas (17) is due to a loss of significant digits in the trigonometric evaluations that involve increasingly large arguments.

Using arbitrary precision arithmetic available in the commercial software package *Mathematica 8*, the loss of precision in stress calculations is illustrated in Fig. 6. If the calculations begin with numerical precision of 500 decimal places, the recursive relations exhibit a linear loss in precision with each recursive step, whereas the explicit analytical solutions exhibit a log-linear loss of precision. Similar conclusions can be made for the recursive and analytical stress solutions at the resonance and non-resonance frequency cases studied here.

3. Continuous forcing function and natural frequencies

In this section, we consider the initial-boundary value problem (3) for a stress loading of the form $\sigma(0, t) = \sin(\omega t)$, for $t \geq 0$. Unlike the discrete model, the stress loading (forcing function) for the continuous model is continuous with time. In addition, unlike the discrete model, the resonance frequency spectrum for the continuous model is not found by solving the corresponding initial-boundary value problem. Instead, we use the linear transformation in frequency

$$\tilde{\omega} = \frac{2\tau}{m}\omega, \tag{27}$$

between the frequency of a continuous forcing function ω and the frequency of the corresponding discrete forcing function $\tilde{\omega}$ and time step $\frac{2\tau}{m}$, to extend the resonance frequency results (19) to our continuous model:

$$\begin{cases} \omega_{l_0} = \dfrac{m}{2\tau}\cdot[\theta_0 + 2l_0\pi] = \dfrac{1}{2\left(\frac{\tau}{m}\right)}\cdot(2l_0+1)\pi, & \text{(for } m \text{ odd only)}, \\ \omega_{l_1,k} = \dfrac{m}{2\tau}\cdot[\theta_k + 2l_1\pi] = \dfrac{1}{2\left(\frac{\tau}{m}\right)}\cdot[\theta_k + 2l_1\pi], & l_0, l_1, l_2 = 0, 1, 2, \ldots, \\ \omega_{l_2,k} = \dfrac{m}{2\tau}\cdot[-\theta_k + 2(l_2+1)\pi] = \dfrac{1}{2\left(\frac{\tau}{m}\right)}\cdot[-\theta_k + 2(l_2+1)\pi], & k = 1, \ldots, \left\lfloor \dfrac{m}{2} \right\rfloor. \end{cases} \tag{28}$$

The linear transformation in frequency (27) is discussed in [28], as the nature of time (continuous or discrete) is expected to affect the nature of the frequency. The frequency for the analog (continuous) time signal is related to the frequency of the digital (discrete) time signal through the linear transformation (27), involving the time step or the so-called sampling interval. For our problem, one can derive relation (27) between the frequency ω of the continuous forcing function $\sin(\omega t)$, $t \geq 0$, and the frequency $\tilde{\omega}$ of the discrete forcing function $\sin(\tilde{\omega} n)$, $n \geq 1$, based on the following operations,

$$\sin(t\omega) = \sin\left(\frac{t}{\frac{2\tau}{m}}\cdot\frac{2\tau}{m}\omega\right) \to \sin\left(\left\lceil\frac{t}{\frac{2\tau}{m}}\right\rceil\cdot\frac{2\tau}{m}\omega\right) = \sin\left(n\cdot\frac{2\tau}{m}\omega\right) = \sin(n\tilde{\omega}).$$

As seen in Fig. 1, $t \geq 0$ represents the time variable, $n = \lceil\frac{t}{\frac{2\tau}{m}}\rceil = 0, 1, 2, \ldots$, represents a time-related index, and $\frac{\tau}{m}$ represents the (equal) wave travel time for each layer.

The proposed resonance frequency spectrum in (28) also represents the natural frequencies of a free-fixed layered strip. The proposed natural frequency formulas in (28) suggest that for a free-fixed m-layered Goupillaud-type strip, the natural frequency spectrum depends on (certain combinations of) the impedance ratios $\alpha_1, \alpha_2, \ldots, \alpha_{m-1}$ and it is inversely proportional to the (equal) wave travel time $\frac{\tau}{m}$ for each layer.

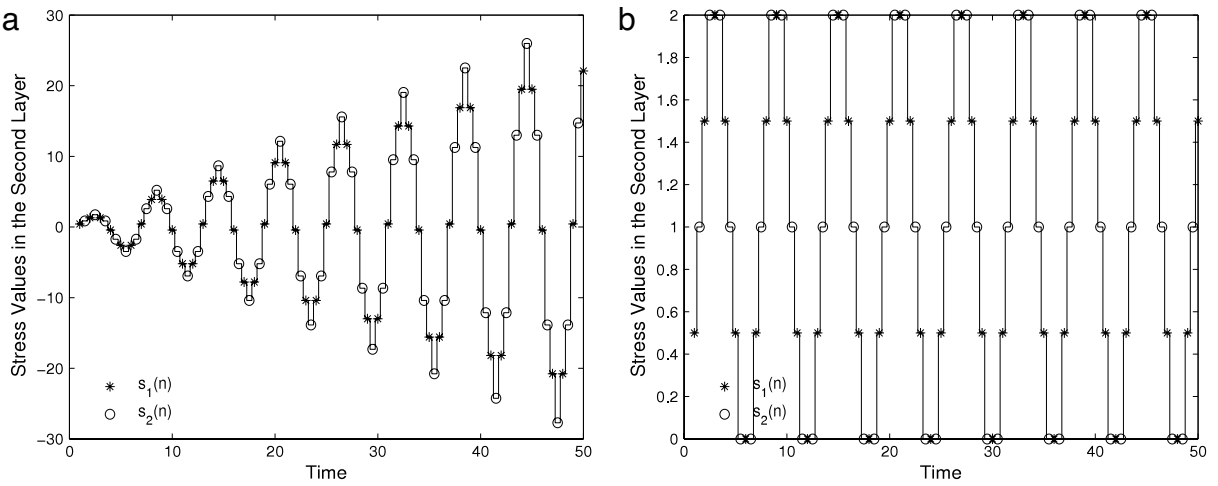

Fig. 7. Stress time history for a two-layered Goupillaud-type strip with impedance ratio $\alpha_1 = 3, \theta_1 = \frac{\pi}{3}, \tau = 1$, at the middle of the second layer located at $\xi = 3/4$ subjected to loading (a) $f(n) = \sin(n\tilde{\omega})$ with $\tilde{\omega} = \theta = \frac{\pi}{3}$. (b) $f(n) = 1$ for $n \geq 0$.

3.1. An alternative derivation of the natural frequency spectrum using the frequency equation

Here, we derive rigorously the natural frequency spectrum (28) for a free-fixed m-layered Goupillaud-type strip, by generalizing the procedure described in [10] and solving the frequency equation for $1 \leq m \leq 5$. Similar to Section 2, the transformation of variables (2) is used to replace the spatial variable x with the travel-time variable ξ for the boundary value problem under consideration. The advantage of applying the transformation of variables (2) is that the frequency equation obtained is a lot simpler to solve, allowing us to recognize patterns and develop formulas for the natural frequency spectrum.

Following the approach taken in Section 2, and applying the transformation of variables (2), the governing equations for $u(\xi, t)$ become:

$$\frac{\partial^2 u_i(\xi,t)}{\partial t^2} = \frac{\partial^2 u_i(\xi,t)}{\partial \xi^2}, \quad \text{for } \xi_{i-1} < \xi < \xi_i,\ i = 1, \ldots, m,$$

where $\xi_0 = 0 < \xi_1 = \frac{\tau}{m} < \xi_2 = \frac{2\tau}{m} < \cdots < \xi_i = \frac{i\tau}{m} < \cdots \xi_m = \tau$, for $i = 1, 2, \ldots, m$. Notice that the wave speed has become unity for each layer, while the material properties become $\tilde{\rho}_i = \tilde{E}_i = \frac{E_i}{c_i} = \sqrt{E_i \rho_i}$ for $i = 1, 2, \ldots, m$, as previously defined in Section 2. Seeking harmonic solutions, we may represent $u(\xi, t) = U(\xi)\psi(t)$ and $U_i(\xi) = A_i \sin\omega\xi + B_i \cos\omega\xi$, for $\xi_{i-1} < \xi < \xi_i$ and $i = 1, \ldots, m$, where ω is the frequency of the harmonic motion. Similarly, $\psi(t)$ can be represented in the form $\psi(t) = A^* \sin\omega t + B^* \cos\omega t$ or in exponential form as $\psi(t) = A^{**} e^{\mathbb{1}\omega t} + B^{**} e^{-\mathbb{1}\omega t}$, where $\mathbb{1} = \sqrt{-1}$. The boundary conditions at $\xi = 0$ and $\xi = \tau$ imply that

$$\frac{\mathrm{d}U_1(0)}{\mathrm{d}\xi} = U_m(\tau) = 0,$$

which together with the continuity of stress and displacement conditions at each layer interface, lead to the following homogeneous linear system of equations,

$$\begin{cases} A_1 = 0, \\ A_i \sin(\omega\xi_i) + B_i \cos(\omega\xi_i) = A_{i+1} \sin(\omega\xi_i) + B_{i+1} \cos(\omega\xi_i) & \text{for } i = 1, \ldots, m-1, \\ \alpha_i [A_i \cos(\omega\xi_i) - B_i \sin(\omega\xi_i)] = A_{i+1} \cos(\omega\xi_i) - B_{i+1} \sin(\omega\xi_i) & \text{for } i = 1, \ldots, m-1, \\ A_m \sin(\omega\xi_m) + B_m \cos(\omega\xi_m) = 0. \end{cases} \tag{29}$$

The relations $\frac{\tilde{E}_i}{\tilde{E}_{i+1}} = \frac{E_i}{c_i} \cdot \frac{c_{i+1}}{E_{i+1}} = \frac{c_i \rho_i}{c_{i+1}\rho_{i+1}} = \alpha_i$, for $i = 1, \ldots, m-1$, were applied to the system (29), using the fact that $c \cdot \rho = E/c$. The system (29) is written in matrix-vector form as

$$\boldsymbol{\Delta}_{\mathbf{m}} \vec{\mathbf{v}} = \vec{\mathbf{0}}, \tag{30}$$

where

$$\boldsymbol{\Delta}_{\mathbf{m}} = \begin{bmatrix} 1 & 0 & 0 & 0 & \dots & 0 \\ \sin\gamma_1 & & & & & \\ \alpha_1\cos\gamma_1 & & & & & \\ 0 & & & & & \\ 0 & & & & & \\ 0 & & & & & \\ \vdots & & & & \tilde{\boldsymbol{\Delta}}_{\mathbf{m}} & \\ & & & & & \\ & & & & & \\ 0 & & & & & \end{bmatrix}_{2m\times 2m}, \qquad \vec{\mathbf{v}} = \begin{bmatrix} A_1 \\ B_1 \\ \vdots \\ A_i \\ B_i \\ \vdots \\ A_m \\ B_m \end{bmatrix}_{2m\times 1}, \tag{31}$$

and

$$\tilde{\boldsymbol{\Delta}}_{\mathbf{m}} = \begin{bmatrix} \cos\gamma_1 & -\sin\gamma_1 & -\cos\gamma_1 & 0 & 0 & 0 & 0 \\ -\alpha_1\sin\gamma_1 & -\cos\gamma_1 & \sin\gamma_1 & 0 & & & \\ 0 & \sin\gamma_2 & \cos\gamma_2 & -\sin\gamma_2 & -\cos\gamma_2 & & \\ 0 & \alpha_2\cos\gamma_2 & -\alpha_2\sin\gamma_2 & -\cos\gamma_2 & \sin\gamma_2 & & \\ & \ddots & \ddots & \ddots & \ddots & \vdots & \vdots \\ 0 & \dots & & & & 0 & 0 \\ 0 & \dots & 0 & \sin\gamma_{m-1} & \cos\gamma_{m-1} & -\sin\gamma_{m-1} & -\cos\gamma_{m-1} \\ 0 & \dots & 0 & \alpha_{m-1}\cos\gamma_{m-1} & -\alpha_{m-1}\sin\gamma_{m-1} & -\cos\gamma_{m-1} & \sin\gamma_{m-1} \\ 0 & \dots & 0 & 0 & 0 & \sin\gamma_m & \cos\gamma_m \end{bmatrix}, \tag{32}$$

with $\gamma_i = \xi_i\omega = \frac{i\tau\omega}{m}$ for $i = 1, \dots, m$. Seeking a nonzero solution for the homogeneous system (30), the determinant of the system matrix $\boldsymbol{\Delta}_{\mathbf{m}}$ must vanish

$$|\boldsymbol{\Delta}_{\mathbf{m}}| = 0. \tag{33}$$

Eq. (33) gives the frequency equation for ω, which can be successfully solved using symbolic algebra software for a strip with up to five layers (see Appendix A). Solving the frequency equation (33) for the general m-layer case, poses a computational challenge.

Comparing the formulas for the natural frequencies from Appendix A with the formulas for the θ-angles from [20], we obtain the following relation,

$$\cos\frac{2\tau}{m}\omega = \cos\theta,$$

which confirms the relationship in (27) between the frequencies $\tilde{\omega}$ given in (19) and ω in (28).

4. Applications of the frequency results

The properties of the materials used in this section are included in Appendix C. The characteristic impedance in each layer is calculated in terms of the material properties $\sqrt{E\rho}$. Once the length of one layer is chosen, the length of each remaining layer is determined according to the recursive relations: $\frac{L_i}{c_i} = \frac{L_{i+1}}{c_{i+1}}$ or $L_{i+1} = \sqrt{\frac{E_{i+1}}{\rho_{i+1}}\cdot\frac{\rho_i}{E_i}}\,L_i$, to provide equal wave travel time. Here L_j, c_j, E_j and ρ_j, for $j = i, i+1$, represent the length, wave speed, elastic modulus and material density for the ith and $(i+1)$th layer respectively, $i = 1, \dots, m-1$.

4.1. One dimensional layered media with a common frequency spectrum

According to (19), the resonance frequency spectrum for the discrete model depends only on certain combinations of the impedance ratios $\alpha_1, \alpha_2, \dots, \alpha_{m-1}$. Such combinations of impedance ratios when $2 \le m \le 5$ are represented by the design parameters χ_{m-1} for $m = 2, 3$, and χ_{m-1}, Γ_{m-1} for $m = 4, 5$, see (10). There are (theoretically) infinitely many m-layered designs of a Goupillaud-type elastic strip that have the same values of the design parameters χ_{m-1}, Γ_{m-1} for $2 \le m \le 5$, and hence the same resonance frequency spectrum for the discrete model.

As for the natural frequency spectrum of a free-fixed m-layered Goupillaud-type strip, based on (28), it depends not only on combinations of the impedance ratios $\alpha_1, \alpha_2, \dots, \alpha_{m-1}$ but also on the (equal) wave travel time $\frac{\tau}{m}$ for each layer. Therefore, to obtain designs with a common natural frequency spectrum, besides having the same values of the relevant design parameters, the layer lengths have to be chosen so that they all have the same wave travel time.

For instance, for the three-layer case with $\chi_2 = (1+\alpha_1)(1+\alpha_2)$, the tungsten–lead–aluminum configuration with $\alpha_1 \approx 5.828$ and $\alpha_2 \approx 0.952$ has the same value of $\chi_2 \approx 13.33$ as the lead–aluminum–copper configuration with $\alpha_1 \approx 0.952$ and $\alpha_2 \approx 5.828$. Another material design with $\chi_2 \approx 13.33$ is the aluminum–steel–brass configuration with $\alpha_1 \approx 0.331$ and $\alpha_2 \approx 9.016$. In addition, in order for these material designs to have a common natural frequency spectrum for the free-fixed strip, only the length of one layer in one of the designs may be chosen at random. The lengths of the remaining layers in all the three designs are then determined to provide equal wave travel time.

4.2. Design modification that gives a desired frequency spectrum within limitations

Adding a new layer in front of an existing two-layered Goupillaud-type strip with $\chi_1 = (1+\alpha_1)$ and θ_1, allows us to modify the resonance frequency spectrum for the discrete model in (19) and (20). The length of the new layer must be chosen so that the strip remains of Goupillaud-type. The new three-layered strip is characterized by $\chi_2 = (1+\alpha_1^*)(1+\alpha_2^*)$ and base angle θ_1^*, with α_1^* to be determined and $\alpha_2^* = \alpha_1$. The unknown impedance ratio α_1^* is derived from the following formula

$$\alpha_1^* = -1 + \frac{2}{\chi_1(1-V)}, \quad \text{where } \frac{\chi_1 - 2}{\chi_1} = \cos\theta_1 < V = \cos\theta_1^* < 1,$$

for a desirable value of the cosine of θ_1^* given by $V = \cos\theta_1^* = \frac{\chi_2 - 2}{\chi_2}$. For instance, for a given $\theta_1 = \frac{\pi}{6}$ and for the choice of $\theta_1^* = \frac{\pi}{9}$ we have that $\cos\theta_1 = \cos\left(\frac{\pi}{6}\right) < V = \cos\theta_1^* = \cos\left(\frac{\pi}{9}\right)$, and the impedance ratios of the three-layered strip are $\alpha_1^* = -1 + \frac{2-\sqrt{3}}{2(1-\cos(\frac{\pi}{9}))}$ and $\alpha_2^* = \frac{2+\sqrt{3}}{2-\sqrt{3}}$. The new natural frequency spectrum is obtained by substituting $\theta_1^* = \frac{\pi}{9}$ into (19) or (20).

4.3. Resonance frequencies and optimal designs

For the m-layered strip subjected to a Heaviside loading [20], it was shown that when the optimal values of the base angles $\theta_{k,opt}$ for $k = 1, \ldots, \lfloor \frac{m}{2} \rfloor$, given in Table B.1 of Appendix B, were substituted into the respective angle-design parameter equations, optimal m-layered designs were generated for $2 \le m \le 5$. These optimal designs were expected to provide the smallest stress amplitude of double the loading in all layers, for all time.

However, when these optimal angle values are substituted into (19) and (28), they generate the resonance frequency spectrum for the discrete and continuous model respectively. As a result, for these designs, depending on the type of loading one can get either the best or the worst outcome when it comes to controlling the stress amplitude, see the illustration in Fig. 7. As the stress amplitude in Fig. 7(a) grows without bound over time for a harmonic forcing condition, the stress amplitude in Fig. 7(b) does not exceed double the loading for a Heaviside loading condition.

4.4. Natural frequencies of a free-fixed non-Goupillaud-type layered strip with integer layer length ratios

The natural frequency results for a free-fixed Goupillaud-type layered strip with equal layer lengths given in (A.1)–(A.7), may be extended to a free-fixed non-Goupillaud-type layered strip with integer layer length ratios.

For instance, the frequency results for a free-fixed four-layered Goupillaud-type strip with equal layer lengths given in (A.5), can be extended to a free-fixed three-layered non-Goupillaud-type strip with wave travel time ratios 1:2:1 by choosing $\alpha_2 = 1$. With these conditions, (A.5) becomes

$$(1+\alpha_1)(1+\alpha_3)\cos^2\frac{\tau}{2}\omega - \Gamma_3\cos\frac{\tau}{2}\omega + (\Gamma_3 - (1+\alpha_1)(1+\alpha_3) + 2) = 0, \tag{34}$$

where $\Gamma_3 = (\alpha_1\alpha_3 - 1)$ is chosen so that the (cosine) solutions vary in the interval $[-1, 1]$. This can be achieved when $\Gamma_3 = 0$, which implies that $(1+\alpha_1)(1+\alpha_3) > 2$. As a result, (34) reduces to:

$$0 < \cos^2\left(\frac{\tau}{2}\omega\right) = \frac{(1+\alpha_1)(1+\alpha_3) - 2}{(1+\alpha_1)(1+\alpha_3)} < 1.$$

5. Conclusions

The resonance frequency spectrum was derived for an m-layered Goupillaud-type elastic medium that was subjected to a discrete, time-harmonic sinusoidal forcing function at one end, and held fixed at the other end. Analytical stress solutions were obtained from a coupled first-order system of difference equations using z-transform methods; key elements of this approach were that the determinant of the resulting global matrix $|\mathbf{A_m}|$ in the z-space was palindromic polynomial with real coefficients, and that its zeros were distinct and on the unit circle. We showed in (19) that the angles $\theta_0 = \pi$ and $\{\pm\theta_k\}_{k=1}^{\lfloor \frac{m}{2} \rfloor}$ corresponding to the zeros of $|\mathbf{A_m}|$ on the unit circle generate the resonance frequency spectrum for the discrete model. The

θ-angle formulas for selected designs can be recovered from (10) and (12)–(14), as well as [20]. In particular, for m odd, the positive angles coterminal with $\theta_0 = \pi$ represent resonance frequencies which do not depend on the material properties. In general, the θ-angles, hence the resonance frequencies for the discrete model, depend only on (certain combinations of) the impedance ratios and not on any other parameters such as the length of the strip, et cetera. According to (19), as long as m-layered designs with different impedance ratios have their θ-angles in common, they are guaranteed to have the same resonance frequency spectrum for the discrete model.

The natural frequency spectrum of a free-fixed m-layered Goupillaud-type strip was derived from the resonance frequency spectrum of the discrete model (19) using the linear transformation for frequencies (27). An alternative derivation was given in Section 3.1 by analytically solving the frequency equation with up to five layers. Based on (28), the natural frequency spectrum of a free-fixed m-layered Goupillaud type strip depends on (combinations of) the impedance ratios and it is inversely proportional to the equal wave travel time for each layer $\frac{\tau}{m}$. Designs with these quantities in common share the same natural frequency spectrum for the free-fixed boundary conditions, see Section 4.1 for illustrations. The transformation of variables (2) was successfully applied in Sections 2 and 3, to simplify the problem under consideration and the frequency equation.

A possible design modification that provides a desired resonance frequency spectrum for the discrete model was demonstrated in Section 4.2. When the resonance frequency results are combined with the stress optimization results obtained in [20], we conclude that for a given optimal design of a Goupillaud-type layered strip with one fixed end, depending on the type of loading at the other end, one can get either the best or the worst outcome when it comes to the stress amplitude. Although this work focused on a Goupillaud-type layered elastic strip, the frequency results were shown to extend to a non-Goupillaud-type layered strip with integer layer length ratios. The stress formulas involving trigonometric sums can also be interpreted using the Chebyshev polynomials of the first and second kind.

So far we have shown that the palindromic polynomial with real coefficients $|\mathbf{A_m}|$ has all its zeros on the unit circle for $1 \leq m \leq 5$, see Section 2.2. Whether this is true for any m-layered Goupillaud-type strip or only for certain classes of designs remains to be investigated. Preliminary work on this topic involving tridiagonal Toeplitz matrices was discussed in Section 2.2. In addition, the experimental validation of the frequency results proposed here would be a natural and valuable extension of this work.

Acknowledgments

We would like to thank Dr. Raymond Wildman at the US Army Research Laboratory, Aberdeen Proving Ground, Maryland, for valuable discussions regarding precision and accuracy of the numerical results presented in this paper. This research effort was partially sponsored by the Short Term Analysis Services (STAS) Pro-gram, administered by the Battelle Memorial Institute in North Carolina for the US Army Research Laboratory under contract No. W911NF-07-D-0001.

Appendix A. Solutions of the frequency equations for a free-fixed m-layered Goupillaud-type elastic strip ($2 \leq m \leq 5$)

A.1. Natural frequency spectrum for the free-fixed two-layer case

After a few mathematical manipulations involving trigonometric identities, the frequency equation (33) for $m = 2$ becomes

$$\cos \tau\omega = \frac{\alpha_1 - 1}{\alpha_1 + 1} = \frac{\chi_1 - 2}{\chi_1}, \quad \text{where } \chi_1 = (1 + \alpha_1) > 1 \text{ or } \alpha_1 > 0. \tag{A.1}$$

This suggests the following natural frequency spectrum

$$\omega_{l_1} = \frac{1}{\tau} \cdot \left[\cos^{-1}\left(\frac{\chi_1 - 2}{\chi_1} \right) + 2l_1\pi \right], \qquad \omega_{l_2} = \frac{1}{\tau} \cdot \left[-\cos^{-1}\left(\frac{\chi_1 - 2}{\chi_1} \right) + 2(l_2 + 1)\pi \right] \tag{A.2}$$

for $l_1, l_2 = 0, 1, 2, \ldots$. Here α_1 represents the impedance ratio between the first and the second layer, while $\chi_1 = 1 + \alpha_1$. When both layers are occupied by the same material ($\alpha_1 = 1$), Eq. (A.1) recovers a known literature result for the natural frequency spectrum of a homogeneous strip of length τ given in [10]. In this case, the frequency equation (A.1) becomes $\cos \tau\omega = 0$ which implies the natural frequency spectrum $\omega_l = \frac{(2l+1)}{\tau} \cdot \frac{\pi}{2}$, $l = 0, 1, 2 \ldots$. Notice that (A.1) implies that $\cos \tau\omega \neq \pm 1$.

A.2. Natural frequency spectrum for the free-fixed three-layer case

Using the fact that $|\boldsymbol{\Delta}_\mathbf{m}| = |\tilde{\boldsymbol{\Delta}}_\mathbf{m}|$, the frequency equation (33) for $m = 3$ becomes equivalent to solving the following equations:

$$\cos \frac{2\tau}{3}\omega = -1 \text{ or } \cos \frac{2\tau}{3}\omega = \frac{\chi_2 - 2}{\chi_2}, \quad \text{where } \chi_2 = (1 + \alpha_1)(1 + \alpha_2) > 1. \tag{A.3}$$

Table B.1
Optimal base angle values for the m-layer case.

m	2	3	4	5
Optimal base angles	$\theta_{1,opt} = \frac{\pi}{j}$	$\theta_{1,opt} = \frac{\pi}{2j-1}$	$\theta_{1,opt} = \frac{\pi}{2j}$, $\theta_{2,opt} = \pi - \frac{\pi}{2j}$	$\theta_{1,opt} = \frac{\pi}{2j+1}$, $\theta_{2,opt} = \frac{(2j-1)\pi}{2j+1}$

From (A.3) the frequency spectrum for the three-layer is

$$\begin{cases} \omega_{l_0} = (2l_0+1)\dfrac{3\pi}{2\tau}, \\ \omega_{l_1} = \dfrac{3}{2\tau}\cdot\left[\cos^{-1}\left(\dfrac{\chi_2-2}{\chi_2}\right)+2l_1\pi\right], \quad \omega_{l_2} = \dfrac{3}{2\tau}\cdot\left[-\cos^{-1}\left(\dfrac{\chi_2-2}{\chi_2}\right)+2(l_2+1)\pi\right], \end{cases} \tag{A.4}$$

where $l_0, l_1, l_2 = 0, 1, 2, \ldots$.

A.3. Natural frequency spectrum for the free-fixed four-layer case

Use of the double angle formula for the cosine for the four-layer case ($m = 4$), results in

$$\cos^2\frac{\tau}{2}\omega - \frac{2\Gamma_3}{\chi_3}\cos\frac{\tau}{2}\omega + \frac{2\Gamma_3-\chi_3+4}{\chi_3} = 0. \tag{A.5}$$

For any given values of the design parameters χ_3 and Γ_3, the frequency spectrum is:

$$\begin{cases} \omega_{l_1} = \dfrac{2}{\tau}\cdot\left[\cos^{-1}\left(\dfrac{\Gamma_3 \pm \sqrt{(\chi_3-\Gamma_3)^2-4\chi_3}}{\chi_3}\right)+2l_1\pi\right], \\ \omega_{l_2} = \dfrac{2}{\tau}\cdot\left[-\cos^{-1}\left(\dfrac{\Gamma_3 \pm \sqrt{(\chi_3-\Gamma_3)^2-4\chi_3}}{\chi_3}\right)+2(l_2+1)\pi\right]. \end{cases} \quad l_1, l_2 = 0, 1, 2\ldots, \tag{A.6}$$

When the first two layers are occupied by one material ($\alpha_1 = 1$) and the other two are occupied by another material ($\alpha_2 \neq 1, \alpha_3 = 1$), the four-layer case reduces to the two-layer case and (A.5) reduces to (A.1). From (A.5) if follows that

$$\cos^2\frac{\tau}{2}\omega = \frac{\alpha_2}{\alpha_2+1},$$

which after applying the double angle formula for cosine becomes consistent with (A.1),

$$\cos\tau\omega = \frac{\alpha_2-1}{\alpha_2+1}.$$

A.4. Natural frequency spectrum for the free-fixed five-layer case

For $m = 5$, $|\boldsymbol{\Delta_5}| = \cos\frac{\tau\omega}{5}\cdot\left[\chi_4\cos^4\frac{\tau}{5}\omega - (\chi_4+\Gamma_4)\cos^2\frac{\tau}{5}\omega + (\Gamma_4+1)\right] = 0$, and we obtain

$$\cos\frac{2\tau}{5}\omega = -1 \text{ or } \cos^2\frac{2\tau}{5}\omega - \frac{2\Gamma_4}{\chi_4}\cos\frac{2\tau}{5}\omega + \frac{2\Gamma_4-\chi_4+4}{\chi_4} = 0. \tag{A.7}$$

The frequency spectrum can then be obtained for any given values of χ_4 and Γ_4, similar to the four layer case.

Appendix B. Optimal base angles

For an m-layered Goupillaud-type elastic strip subjected to a Heaviside loading at one end and held fixed at the other end, the optimal designs have the smallest stress amplitude of double the loading. These optimal designs are characterized by the optimal values in Table B.1 of their base angles for $j = 2, 3, 4, \ldots$:

Appendix C. Material properties

The elastic modulus E and density ρ of the materials used in Section 4.1 (see [29]) are as follows:
Aluminum alloy: $E = 70$ GPa and $\rho = 2500$ kg/m^3; Brass: $E = 20$ GPa and $\rho = 984.19$ kg/m^3; Copper alloy: $E = 10$ GPa and $\rho = 515.19$ kg/m^3; Lead: $E = 14$ GPa and $\rho = 11,340$ kg/m^3; Tungsten alloy: $E = 275$ GPa and $\rho = 19,610$ kg/m^3; Steel: $E = 200$ GPa and $\rho = 8000$ kg/m^3.

References

[1] W. Broer, B.J. Hoenders, Natural modes and resonances in a dispersive stratified N-layer medium, J. Phys. A-Math. Theor. 42 (24) (2009) 245207.
[2] A.I. Fedorchenko, I. Stachiv, A.-B. Wang, W.-H. Wang, Fundamental frequencies of mechanical systems with N-piecewise constant properties, J. Sound Vibr. 317 (2008) 490–495.
[3] W. Hsueh, Analytical solution of harmonic travelling waves in N-segment strings, Proc. R. Soc. Lond. Ser. A-Math. Phys. Eng. Sci. 456 (2000) 2115–2126.
[4] S. Gaudet, C. Gauthier, V.G. LeBlanc, On the vibrations of an N-string, J. Sound Vibr. 238 (1) (2000) 147–169.
[5] R.R. Churchill, Operational Mathematics, McGraw-Hill, New York, 1972.
[6] G. Caviglia, A. Morro, A closed-form solution for reflection and transmission of transient waves in multilayers, J. Acoust. Soc. Am. 116 (2) (2004) 643–654.
[7] J. Kaplunov, A. Krynkin, Resonance vibrations of an elastic interfacial layer, J. Sound Vibr. 294 (2006) 663–677.
[8] G. Qiang, Z. Wanxie, W.P. Howson, A precise method for solving wave propagation problems in layered anisotropic media, Wave Motion 40 (2004) 191–207.
[9] M.S. Fokina, V.N. Fokin, Resonances of acoustic waves interacting with an elastic seabed, J. Comput. Acoust. 9 (3) (2001) 1079–1093.
[10] K.F. Graff, Wave Motion in Elastic Solids, Dover Publications, New York, 1975.
[11] J.F. Claerbout, Fundamentals of Geophysical Data Processing: With Applications to Petroleum Processing, McGraw-Hill, New York, 1976.
[12] P. Goupillaud, An approach to inverse filtering of near-surface layer effects from seismic records, Geophysics 36 (1961) 754–760.
[13] M.A. Hooshyar, Goupillaud layers and construction of wave speed and density of a layered acoustic medium, J. Acoust. Soc. Am. 87 (6) (1990) 2310–2313.
[14] R. Courant, D. Hilbert, Methods of Mathematical Physics, vol. 1, Interscience, New York, 1953.
[15] J.A. Ware, K. Aki, Continuous and discrete inverse-scattering problems in a stratified elastic medium I. Plane waves at normal incidence, J. Acoust. Soc. Am. 45 (4) (1969) 911–921.
[16] L. Knopoff, A matrix method for elastic wave problems, Bull. Seismol. Soc. Am. 54 (1964) 431–438.
[17] N.A. Haskell, The dispersion of surface waves on multilayered media, Bull. Seismol. Soc. Amer. 43 (1953) 1734.
[18] W.T. Thomson, Transmission of elastic waves through a stratified solid medium, J. Appl. Phys. 21 (1950) 8993.
[19] K. Bube, R. Burridge, The one dimensional inverse problem of reflection seismology, SIAM Rev. 25 (4) (1983) 497–559.
[20] A.P. Velo, G.A. Gazonas, T. Ameya, z-transform methods for the optimal design of one-dimensional layered elastic media, SIAM J. Appl. Math. 70 (3) (2009) 762–788.
[21] E.I. Jury, Theory and Application of the z-Transform Method, John Wiley & Sons, 1964.
[22] P.R. Parthasarathy, S. Dharmaraja, The transient solution of a local-jump heterogeneous chain in diatomic systems, J. Phys. A: Math. Gen. 31 (1998) 6579–6588.
[23] A. Bultheel, P. Gonzalez-Vera, E. Hendriksen, O. Njastad, Orthogonal rational functions and tridiagonal matrices, J. Comput. Appl Math. 153 (2003) 89–97.
[24] A.R. Willms, Analytical results for the eigenvalues of certain tridiagonal matrices, SIAM J. Matrix Anal. Appl. 30 (2) (2008) 639–656.
[25] C.M. da Fonseca, The characteristic polynomial of some perturbed tridiagonal k-Toeplitz matrices, Appl. Math. Sci. 1 (2) (2007) 59–67.
[26] R. Alvarez-Nodarse, J. Petronilho, N.R. Quintero, On some tridiagonal k-Toeplitz matrices: algebraic and analytical aspects. Applications, J. Comput. Appl Math. 184 (2005) 518–537.
[27] W.L. Oberkampf, C.J. Roy, Verification and Validation in Scientific Computing, Cambridge University Press, 2010.
[28] J.G. Proakis, D.G. Manolakis, Introduction to Digital Signal Processing, Macmillan Publishing Company, 1988.
[29] M.F. Ashby, Materials Selection in Mechanical Design, second ed., Butterworth-Heinemann, Oxford, UK, 2000.

NO. OF COPIES	ORGANIZATION
1 (PDF only)	DEFENSE TECHNICAL INFORMATION CTR DTIC OCA 8725 JOHN J KINGMAN RD STE 0944 FORT BELVOIR VA 22060-6218
1	DIRECTOR US ARMY RESEARCH LAB IMNE ALC HRR 2800 POWDER MILL RD ADELPHI MD 20783-1197
1	DIRECTOR US ARMY RESEARCH LAB RDRL CIO LL 2800 POWDER MILL RD ADELPHI MD 20783-1197
1	DIRECTOR US ARMY RESEARCH LAB RDRL CIO LT 2800 POWDER MILL RD ADELPHI MD 20783-1197
1	DIRECTOR US ARMY RESEARCH LAB RDRL D 2800 POWDER MILL RD ADELPHI MD 20783-1197

NO. OF COPIES ORGANIZATION

2 NSF
S MCKNIGHT
G PAULINO
4201 WILSON BLVD STE 545
ARLINGTON VA 22230-0002

2 DARPA
W COBLENZ
J GOLDWASSER
3701 N FAIRFAX DR
ARLINGTON VA 22203-1714

2 US ARMY TARDEC
AMSTRA TR R MS 263
K BISHNOI
D TEMPLETON MS 263
WARREN MI 48397-5000

1 DIRECTOR
US ARMY ARDEC
AMSRD AAR AEE W
E BAKER
BLDG 3022
PICATINNY ARSENAL NJ
07806-5000

1 COMMANDER
US ARMY RSRCH OFC
RDRL ROI M
J LAVERY
PO BOX 12211
RESEARCH TRIANGLE PARK NC
27709-2211

1 COMMANDER
US ARMY RSRCH OFC
RDRL ROE M
D STEPP
PO BOX 12211
RESEARCH TRIANGLE PARK NC
27709-221

5 SOUTHWEST RSRCH INST
C ANDERSON
K DANNEMANN
T HOLMQUIST
G JOHNSON
J WALKER
PO DRAWER 28510
SAN ANTONIO TX 78284

NO. OF COPIES ORGANIZATION

1 ERDC
US ARMY CORPS OF ENGINEERS
USACEGSL
P PAPADOS
7701 TELEGRAPH RD
ALEXANDRIA VA 22315

1 AFOSR/NL
875 NORTH RANDOLPH ST
SUITE 325 RM 3112
F FAHROO
ARLINGTON VA 22203

5 NAVAL RESEARCH LAB
E R FRANCHI CODE 7100
M H ORR CODE 7120
J A BUCARO CODE 7130
J S PERKINS CODE 7140
S A CHIN BING CODE 7180
4555 OVERLOOK AVE SW
WASHINGTON DC 20375

1 UNIV OF MISSISSIPPI
DEPT OF MECH ENGRG
A M RAJENDRAN
201-B CARRIER HALL
UNIVERSITY MS 38677

2 SRI INTERNATIONAL
D CURRAN
D SHOCKEY
333 RAVENSWOOD AVE
MENLO PARK CA 94025

1 VIRGINIA POLYTECHNIC INST
COLLEGE OF ENGRG
R BATRA
BLACKSBURG VA 24061-0219

1 JOHNS HOPKINS UNIV
DEPT OF MECH ENGRG
K T RAMESH
LATROBE 122
BALTIMORE MD 21218

1 INST OF ADVANCED TECH
UNIV OF TX AUSTIN
S BLESS
3925 W BRAKER LN STE 400
AUSTIN TX 78759-5316

NO. OF COPIES ORGANIZATION

1 APPLIED RSCH ASSOCIATES
D E GRADY
4300 SAN MATEO BLVD NE
STE A220
ALBUQUERQUE NM 87110

1 INTERNATIONAL RSRCH
ASSOC INC
D L ORPHAL CAGE 06EXO
4450 BLACK AVE
PLEASANTON CA 94566

2 WASHINGTON ST UNIV
INST OF SHOCK PHYSICS
Y M GUPTA
J ASAY
PULLMAN WA 99164-2814

1 UNIV OF DAYTON
RSRCH INST
N S BRAR
300 COLLEGE PARK
MS SPC 1911
DAYTON OH 45469

1 TEXAS A&M UNIV
DEPT OF GEOLOGY &
GEOPHYSICS MS 3115
F CHESTER
COLLEGE STATION TX 778431

1 UNIV OF SAN DIEGO
DEPT OF MATH & CMPTR SCI
A VELO
5998 ALCALA PARK
SAN DIEGO CA 92110

1 NATIONAL INST OF
STANDARDS & TECHLGY
BLDG & FIRE RSRCH LAB
J MAIN
100 BUREAU DR MS 8611
GAITHERSBURG MD 20899-8611

1 MIT
DEPT ARNTCS ASTRNTCS
R RADOVITZKY
77 MASSACHUSETTS AVE
CAMBRIDGE MA 02139

1 PENN STATE UNIV
DEPT OF ENGRG SCI & MECH
F COSTANZO
UNIVERSITY PARK PA 168023

NO. OF COPIES ORGANIZATION

1 UNIV OF TEXAS-PAN AMERICAN
COLLEGE OF ENGRG
& COMPUTER SCI
D H ALLEN
1201 WEST UNIVERSITY DR
EDINBURG, TX 78539-2999

1 CLEMSON UNIV
DEPT OF MECH ENGRG
M GRUJICIC
241 ENGRG INNOVATION BLDG
CLEMSON SC 29634-0921

1 UNIV OF DELAWARE
DEPT ELECTRICAL & CMPTR
ENGRG
D WEILE
NEWARK DE 19716

7 UNIV OF NEBRASKA
DEPT OF ENGRG MECH
F BOBARU
Y DZENIS
G GOGOS
M NEGAHBAN
R FENG
J TURNER
Z ZHANG
LINCOLN NE 68588

1 WORCESTER POLYTECHNIC INST
MATHEMATICAL SCI
K LURIE
WORCESTER MA 01609

4 UNIV OF UTAH
DEPT OF MATH
A CHERKAEV
E CHERKAEV
E S FOLIAS
R BRANNON
SALT LAKE CITY UT 84112

4 UNIV OF DELAWARE
DEPT OF MECH ENGRG
T BUCHANAN
T W CHOU
A KARLSSON
M SANTARE
126 SPENCER LAB
NEWARK DE 19716

NO. OF
COPIES ORGANIZATION

1 NORTHWESTERN UNIV
DEPT OF CIVIL & ENVIRON ENGRG
Z BAZANT
2145 SHERIDAN RD A135
EVANSTON IL 60208-3109

1 UNIV OF DELAWARE
CTR FOR COMPST MATRLS
J GILLESPIE
NEWARK DE 19716

1 LOUISIANA STATE UNIV
R LIPTON
304 LOCKETT HALL
BATON ROUGE LA 70803-4918

1 UNIV OF ILLINOIS
DEPT OF MECHL SCI & ENGRG
A F VAKAKIS
1206 W GREEN ST MC 244
URBANA CHAMPAIGN IL 61801

1 UNIV OF ILLINOIS
ARSPC ENGRG
J LAMBROS
104 S WRIGHT ST MC 236
URBANA CHAMPAIGN IL 61801

1 T W WRIGHT
4906 WILMSLOW RD
BALTIMORE MD 21210

4 ADELPHI LABORATORY CTR
C CHABALOWSKI
J CHANG
O OCHOA
R SKAGGS
BLDG 205
2800 POWDER MILL RD
ADELPHI MD 20783-1197

ABERDEEN PROVING GROUND

89 DIR USARL
RDRL CIH C
J CAZAMIAS
P CHUNG
D GROVE
J KNAP
RDRL WM
B FORCH
S KARNA
J MCCAULEY
P PLOSTINS
RDRL WML
J NEWILL
M ZOLTOSKI
RDRL WML B
I BATYREV
S IZVYEKOV
B RICE
R PESCE RODRIGUEZ
D TAYLOR
N TRIVEDI
N WEINGARTEN
RDRL WML D
P CONROY
M NUSCA
RDRL WML E
P WEINACHT
RDRL WML F
D LYON
RDRL WML G
M BERMAN
W DRYSDALE
RDRL WML H
D SCHEFFLER
S SCHRAML
B SCHUSTER
RDRL WMM
J BEATTY
R DOWDING
J ZABINSKI
RDRL WMM A
J SANDS
J TZENG
E WETZEL
RDRL WMM B
T BOGETTI
B CHEESEMAN
C FOUNTZOULAS
G GAZONAS
D HOPKINS
R KARKKAINEN
P MOY
B POWERS
C RANDOW
T SANO
F TAVAZZA
M VANLANDINGHAM
R WILDMAN
C YEN
RDRL WMM C
J LA SCALA
RDRL WMM D
E CHIN
K CHO

NO. OF
COPIES ORGANIZATION

RDRL WMM E
J ADAMS
M COLE
T JESSEN
J LASALVIA
P PATEL
J SINGH
RDRL WMM F
L KECSKES
H MAUPIN
RDRL WML G
J ANDZELM
A RAWLETT
RDRL WMP
P BAKER
S SCHOENFELD
RDRL WMP A
B RINGERS
RDRL WMP B
C HOPPEL
R KRAFT
S SATAPATHY
M SCHEIDLER
T WEERASOORIYA
RDRL WMP C
R BECKER
S BILYK
T BJERKE
D CASEM
J CLAYTON
M GREENFIELD
B LEAVY
M RAFTENBERG
S SEGLETES
RDRL WMP D
R DONEY
D KLEPONIS
J RUNYEON
B SCOTT
H MEYER
RDRL WMP E
M BURKINS
B LOVE
RDRL WMP F
A FRYDMAN
N GNIAZDOWSKI
R GUPTA
RDRL WMP G
N ELDREDGE
D KOOKER
S KUKUCK